Monocytes, neutrophils, and platelets cooperate to initiate and propagate venous thrombosis in mice in vivo

Marie-Luise von Brühl,[1,4] Konstantin Stark,[1,4] Alexander Steinhart,[1,4]
Sue Chandraratne,[1,4] Ildiko Konrad,[1,4] Michael Lorenz,[1,4]
Alexander Khandoga,[1,4] Anca Tirniceriu,[1,4] Raffaele Coletti,[1,4]
Maria Köllnberger,[1,4] Robert A. Byrne,[1,4] Iina Laitinen,[2] Axel Walch,[5]
Alexander Brill,[6] Susanne Pfeiler,[7] Davit Manukyan,[7] Siegmund Braun,[1]
Philipp Lange,[8] Julia Riegger,[1,4] Jerry Ware,[9] Annekathrin Eckart,[1,4]
Selgai Haidari,[1,4] Martina Rudelius,[3] Christian Schulz,[1,4,10]
Katrin Echtler,[1,4] Volker Brinkmann,[11] Markus Schwaiger,[2]
Klaus T. Preissner,[12] Denisa D. Wagner,[6] Nigel Mackman,[13]
Bernd Engelmann,[7] and Steffen Massberg[1,4]

[1]Deutsches Herzzentrum and I. Medizinische Klinik, [2]Nuklearmedizinische Klinik und Poliklinik, Klinikum rechts der Isar, and [3]Institut für Allgemeine Pathologie und Pathologische Anatomie, Technische Universität München (TUM), 80333 Munich, Germany
[4]Munich Heart Alliance, Munich, Germany
[5]Helmholtz Zentrum München, Deutsches Forschungszentrum für Umwelt und Gesundheit, Institut für Pathologie, 85764 Neuherberg, Germany
[6]Immune Disease Institute, Program in Cellular and Molecular Medicine, Children's Hospital, Boston, and Department of Pediatrics, Harvard Medical School, Boston, MA 02115
[7]Institut für Klinische Chemie and [8]Medizinische Klinik I, Ludwig-Maximilians-Universität, 81377 Munich, Germany
[9]Department of Physiology and Biophysics, University of Arkansas for Medical Sciences, Little Rock, AR 72205
[10]Centre for Molecular and Cellular Biology of Inflammation, King's College London, London SE1 1UL, UK
[11]Max-Planck-Institut für Infektionsbiologie, 10117 Berlin, Germany
[12]Department of Biochemistry, University of Giessen, 35392 Giessen, Germany
[13]Department of Medicine, University of North Carolina at Chapel Hill, Chapel Hill, NC 27514

CORRESPONDENCE
Steffen Massberg:
massberg@idi.harvard.edu

Abbreviations used: DVT, deep vein thrombosis; GP, glycoprotein; IVC, inferior vena cava; MPO, myeloperoxidase; NE, neutrophil elastase; NET, neutrophil extracellular trap; TF, tissue factor; VTE, venous thromboembolism; vWF, von Willebrand factor.

Deep vein thrombosis (DVT) is a major cause of cardiovascular death. The sequence of events that promote DVT remains obscure, largely as a result of the lack of an appropriate rodent model. We describe a novel mouse model of DVT which reproduces a frequent trigger and resembles the time course, histological features, and clinical presentation of DVT in humans. We demonstrate by intravital two-photon and epifluorescence microscopy that blood monocytes and neutrophils crawling along and adhering to the venous endothelium provide the initiating stimulus for DVT development. Using conditional mutants and bone marrow chimeras, we show that intravascular activation of the extrinsic pathway of coagulation via tissue factor (TF) derived from myeloid leukocytes causes the extensive intraluminal fibrin formation characteristic of DVT. We demonstrate that thrombus-resident neutrophils are indispensable for subsequent DVT propagation by binding factor XII (FXII) and by supporting its activation through the release of neutrophil extracellular traps (NETs). Correspondingly, neutropenia, genetic ablation of FXII, or disintegration of NETs each confers protection against DVT amplification. Platelets associate with innate immune cells via glycoprotein Ibα and contribute to DVT progression by promoting leukocyte recruitment and stimulating neutrophil-dependent coagulation. Hence, we identified a cross talk between monocytes, neutrophils, and platelets responsible for the initiation and amplification of DVT and for inducing its unique clinical features.

M.-L. von Brühl and K. Stark contributed equally to this paper.

Deep vein thrombosis (DVT) and pulmonary embolism, collectively referred to as venous thromboembolism (VTE), constitute a leading cause of cardiovascular death (Roger et al., 2011). The incidence of VTE increases dramatically over 45 yr of age and ranges from 300,000 to more than two million per year in the United States with similar rates in Europe (Cohen et al., 2007; Heit, 2008; Moll and Mackman, 2008). In light of an increasing life expectancy, strategies to prevent and treat VTE will become an even more important health care issue worldwide (Silverstein et al., 1998). Whereas arterial thrombosis is triggered by endothelial disruption, a frequent mechanism leading to DVT is stasis in the absence of endothelial injury (Sevitt, 1970; Esmon, 2009). In keeping with this, immobilization (e.g., during long-distance flights), pregnancy, and chronic venous insufficiency, each major causes of impaired venous blood flow, are associated with an increased risk of DVT development (Payling Weight et al., 1951; Wright et al., 1952; Geerts et al., 1994; Hughes et al., 2003; Heit et al., 2005). However, the molecular and cellular events that translate depressed venous blood flow into thrombogenesis remain unknown.

Venous thrombi have a characteristic laminar structure. They are rich in fibrin and red blood cells and they are pervaded by large numbers of leukocytes (Wakefield et al., 1995). There is increasing evidence that inflammatory processes and DVT are closely linked. In support of this, C-reactive protein, an inflammatory marker, has been shown to be increased in DVT patients. In addition, acute infections predispose to DVT, further supporting a role of inflammation in thrombosis (Bucek et al., 2002; Smeeth et al., 2006). Whereas several studies have implicated leukocytes in DVT resolution, their role in DVT development, as well as the precise contribution of different leukocyte subsets to DVT induction, still remains unclear.

In particular, the lack of an appropriate mouse model leading to DVT in a large vein without applying endothelial denudation has limited our understanding of the processes that support different stages of venous thrombogenesis. We therefore established a novel mouse model of DVT induced by flow restriction, closely resembling the kinetics, the histological features, and the clinical presentation of human DVT in patients with compromised venous blood flow. Using this model in combination with state-of-the-art intravital imaging, we assessed the early cellular events that trigger DVT formation. We identified that reduction of blood flow induces a proinflammatory endothelial phenotype initiating recruitment of innate immune cells, particularly neutrophils and monocytes. Recruited leukocytes start fibrin formation via blood cell–derived tissue factor (TF), which, as we show here, is the decisive trigger for the massive fibrin deposition characteristic of DVT. Furthermore, platelets are critical for DVT propagation, as they support leukocyte accumulation and promote neutrophil extracellular trap (NET) formation, which in turn triggers FXII-dependent thrombus propagation.

RESULTS

Flow restriction in mice induces venous thrombosis resembling human DVT

Most of our current mechanistic knowledge regarding DVT pathophysiology has been gained from mouse models using denudation of the venous endothelial surface (Eitzman et al., 2000; Angelillo-Scherrer et al., 2001; Wang et al., 2006). However, unlike in arterial thrombosis, a frequent (though not the only) trigger for DVT formation in patients is depression of venous blood flow without endothelial denudation (Sevitt, 1974; Mammen, 1992). To account for this common clinical setting leading to DVT in humans, we developed a novel mouse model in which venous thrombosis is initiated by restriction of blood flow in the absence of endothelial disruption, as indicated by scanning electron microscopy (Fig. 1 A). When we reduced blood flow in the inferior vena cava (IVC) by ∼80% (Fig. 1 B), we detected small thrombi across different mouse strains after 6–12 h, whereas completely occlusive thrombi developed beyond 24–48 h in 60% of mice (not depicted; and Fig. 1, C and D). This protracted time course of DVT development closely resembles the dynamics of human DVT formation (Warlow et al., 1976). Computed tomography revealed DVT in mice with flow restriction, but not in sham-operated animals (Fig. 1 C and Video 1), excluding surgical trauma as a trigger. Thrombogenesis was restricted to the IVC, whereas systemic thrombus formation was not observed. Similar to human VTE, mouse DVT development could be prevented by enoxaparin (Fig. 1 D). Mature thrombi revealed the characteristic layered morphology reminiscent of thrombi in DVT patients with a larger red thrombus and a smaller proportion of white thrombus material (Fig. 1, E and F; Sevitt, 1974). Together, this suggests that our DVT model closely reproduces the time course, histological features, and clinical presentation of localized DVT in humans, developing in response to reduced venous blood flow.

Innate immune cells are recruited to the vessel wall early during DVT formation

Although recent studies have suggested a link between inflammation and DVT, the precise role of immune cells in DVT development remains unclear (Day et al., 2005; Roumen-Klappe et al., 2009). When we examined venous thrombi that developed in response to 48 h of flow restriction, inflammatory leukocytes were in fact a major cellular constituent. Leukocytes were distributed in clusters or layers adjacent to the intact endothelium (Fig. 1 F, Fig. 2 A, and Video 2). Ly6G^{hi} myeloperoxidase (MPO)-expressing neutrophils were the predominant leukocyte subset within venous thrombi constituting ∼70% of all accumulated leukocytes, whereas Ly6G$^-$F4/80$^+$ monocytes represented the remainder, ∼30% (Fig. 2 A and not depicted). Lymphocytes were virtually absent, pointing to the active accumulation of myeloid leukocytes in mouse DVT.

We then determined whether accumulation of innate immune cells is a consequence or rather a cause of DVT formation. Scanning and transmission electron microscopy, as well
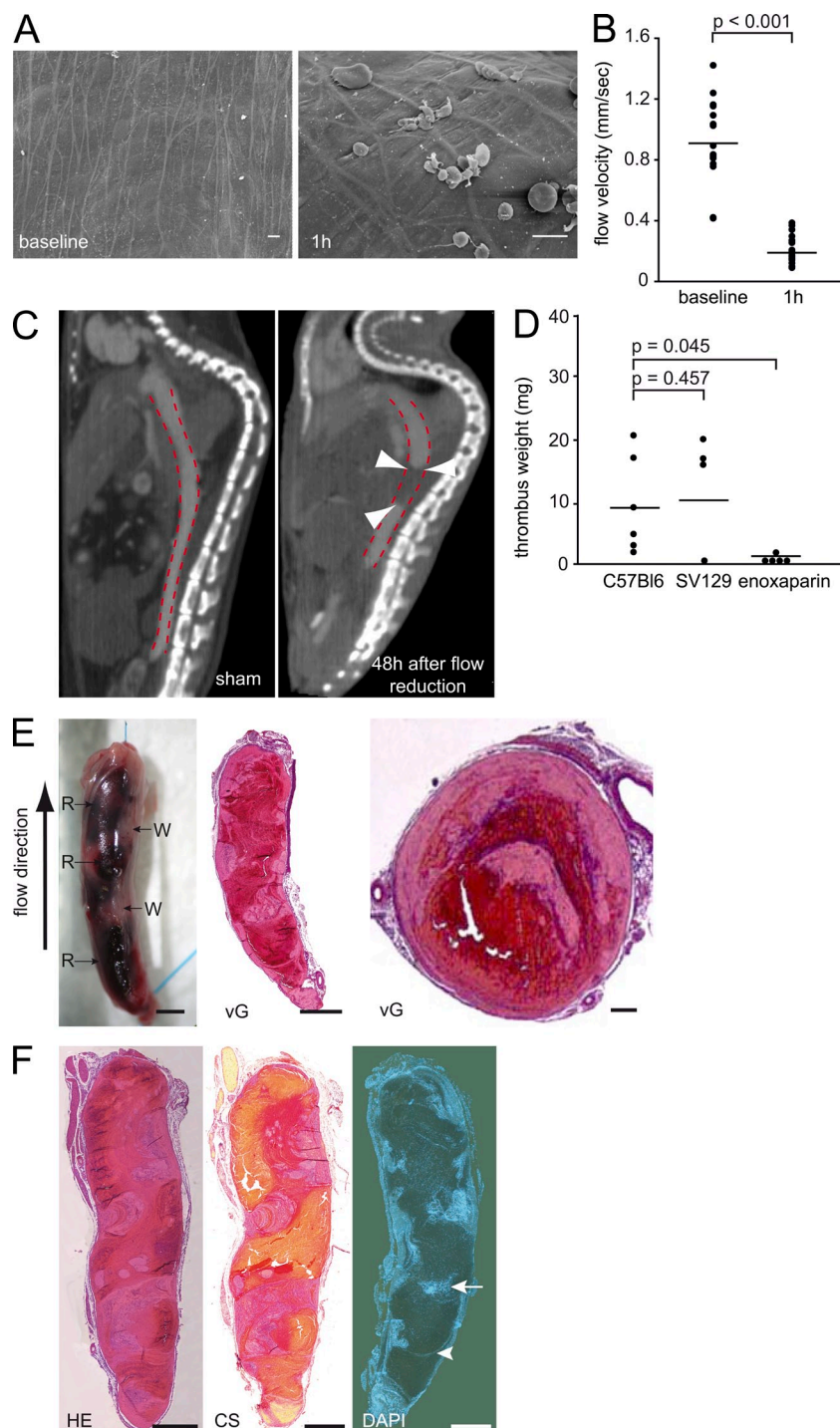
Figure 1. A novel clinically relevant mouse model of DVT. (A) Scanning electron microscopic images of the IVC. Images taken immediately after (baseline) and 1 h after partial ligation in the IVC illustrate the intact endothelial cell lining of the IVC without endothelial disruption. Bars, 5 µm. Shown is a representative of $n = 3$ experiments. (B) Assessment of blood flow in the IVC in response to partial ligation ($n = 16$). Dots represent individual experiments; lines show the mean of each group. (C) Evaluation of DVT by contrast-enhanced computed tomography (CT) 48 h after flow restriction in the IVC (also see Video 1). CT images were acquired in a sagittal projection using a small animal CT scanner. Right: animal with DVT at 48 h after flow restriction. The dotted line shows the IVC in the abdominal cavity. Arrowheads point to the lack of contrast agent, indicating thrombus formation. Left: control animal with sham ligation showing continuous contrast filling of the IVC. Shown is a representative of $n = 3$ experiments. (D) Weight (milligrams) of harvested IVC thrombi 48 h after DVT induction in C57BL/6 ($n = 6$), SV129 mice ($n = 4$), and after enoxaparin treatment ($n = 5$). Dots represent individual experiments; lines show the mean of each group. (E) Macroscopic and microscopic assessment of venous thrombi after 48 h of flow restriction in C57BL/6 animals. Regions of red (R) and white (W) thrombus can be distinguished macroscopically (left) and microscopically in a longitudinal (middle) and cross section (right) stained with van Gieson (vG). The thrombus shows the typical white and erythrocyte-rich red layers. Bars: (left and middle) 1 mm; (right) 100 µm. Shown is a representative of $n = 10$ experiments. (F) Excised thrombosed IVC obtained 48 h after induction of DVT in C57BL/6 animals. Regions of red and white thrombus can be distinguished microscopically in a longitudinal HE-stained section. Carstairs staining (CS) is demonstrating the layers of fibrin, platelets, and red blood cells throughout the thrombus, and DAPI staining illustrates the distribution of leukocytes in clusters (arrow) and layers (arrowhead). Bars, 1 mm. Shown is a representative of $n = 3$ experiments.

as standard histology, revealed that leukocytes were recruited to the IVC in large quantities already after 6 h of flow restriction (Fig. 2, B–D). Leukocytes adhered directly to the luminal aspect of the venous endothelium, whereas endothelial disruption was never detected (Fig. 2, B–D). Next, we performed intravital epifluorescence and two-photon microscopy (2P-IVM) to dissect the dynamics of leukocyte recruitment during DVT development in the IVC in response to flow restriction. Within only 1 h of depressed venous blood flow, leukocytes started to roll along, adhere, or crawl on the venous endothelium (Fig. 3, A–C; and Video 3). In contrast, leukocytes barely interacted with the endothelium when venous blood flow was left unperturbed in sham-operated animals, excluding surgical preparation as trigger of the inflammatory response (unpublished data). Leukocyte accumulation increased significantly over time, and after 5–6 h leukocytes carpeted virtually the entire endothelial surface (Fig. 3, B and C), consistent with the ex vivo observations (Fig. 2, B–D). These findings clearly suggest that massive leukocyte accumulation precedes the development of DVT in response to restriction of venous blood flow.
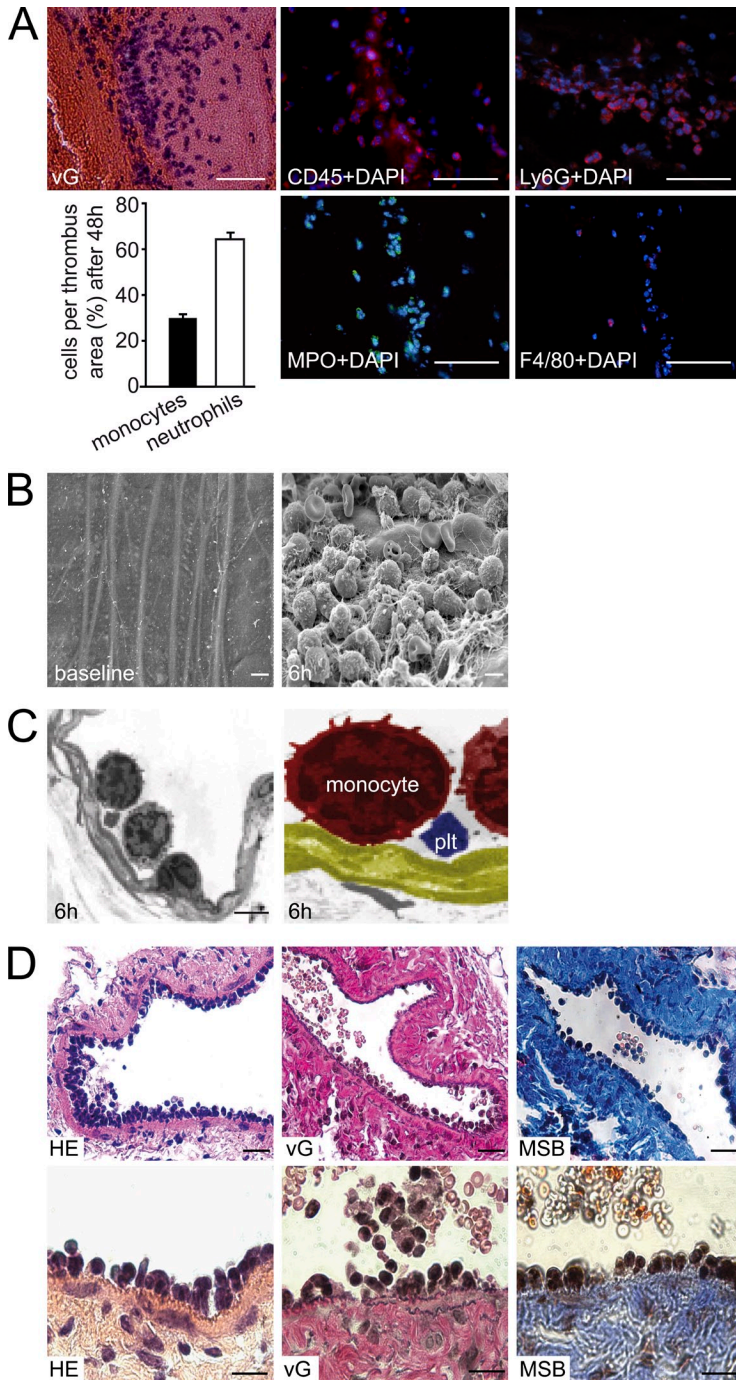
**Figure 2. Leukocytes are recruited during the early phase of venous thrombosis to the intact endothelial surface.** (A) Leukocyte accumulation in DVT induced by 48 h of flow restriction. vG (top left) and immunohistochemical stainings (middle and right, top and bottom) for Ly6G+ MPO+ neutrophils and F4/80+ monocytes. Nuclei are counterstained with DAPI. Bars, 50 µm. The bottom left shows the quantification of neutrophils and monocytes. Results are mean ± SEM ($n = 3$). (B) Scanning electron microscopic images taken directly after partial IVC ligation showing the intact endothelium. After 6 h, a carpet composed of cell aggregates and fibrin can be visualized on the endothelial surface. Bars, 5 µm. (C) TEM images of venous vessels showing the anticoagulant endothelial cell lining (pseudocolored in yellow). Bar, 5 µm. Detail is shown in the right image. (D) Histological analyses of the IVC 6 h after flow reduction examining leukocyte recruitment in the early phase of venous thrombus formation. Histological sections in three different stainings (HE, vG, and MSB). Bars: (top row) 20 µm; (bottom row) 10 µm. Data are representative of $n = 3$ experiments per group.

and Video 4). We then examined heterozygous CX₃CR1–eGFP mice to specifically define monocyte recruitment. This revealed that CX₃CR1+ monocytes constitute ∼15% of the recruited leukocytes (Fig. 3, D and F; and Video 5). Together, these findings indicate that neutrophils and monocytes are the predominant leukocyte subsets that actively accumulate at the vascular surface during DVT development.

Leukocyte accumulation depends on endothelial P-selectin

Subsequently, we evaluated the molecular determinants triggering the accumulation of leukocytes during DVT development. Flow restriction resulted in up-regulation of mRNA encoding for multiple trafficking molecules, including CCL2, CXCL1, CXCL5, and IL-6 (Fig. 4 A). In addition, the endothelium of the restricted IVC was decorated with P-selectin and von Willebrand factor (vWF), two adhesive proteins stored in endothelial Weibel Palade bodies and mobilized to the endothelial surface upon cell activation (Myers et al., 2002). In contrast, P-selectin mRNA was only moderately (nonsignificantly) up-regulated (Fig. 4, B and C). This suggests that in response to depressed blood flow, the vessel wall adopts a proinflammatory phenotype with intact but activated endothelial cells exposing adhesion molecules on their surfaces. We then focused on the role of P-selectin (Fig. 4, B and C). In P-selectin–deficient mice ($SELP^{-/-}$), leukocyte rolling (not depicted) and subsequent adhesion was virtually absent (Fig. 4 D). Notably, $SELP^{-/-}$ mice were protected against DVT development (Fig. 4 E), indicating that recruitment of innate immune cells is indispensable for DVT development. Both platelets and endothelial cells express P-selectin; however, infusion of WT platelets into $SELP^{-/-}$ mice did not rescue

To dissect the leukocyte subsets recruited in response to depressed blood flow, we next induced flow restriction in LysM-eGFP reporter mice. We observed that >80% of all cells recruited during the first 6 h were eGFP^hi (Fig. 3 D). In addition to neutrophils, monocytes also express eGFP in LysM-eGFP mutants, albeit at lower levels that are beyond the detection limit of 2P-IVM (Fig. 3 E). Correspondingly, 2P-IVM revealed that ∼90% of all eGFP^hi cells recruited to venous thrombi also stain positive for Ly6G, indicating that eGFP^hi cells indeed mainly represent neutrophils (Fig. 3 F
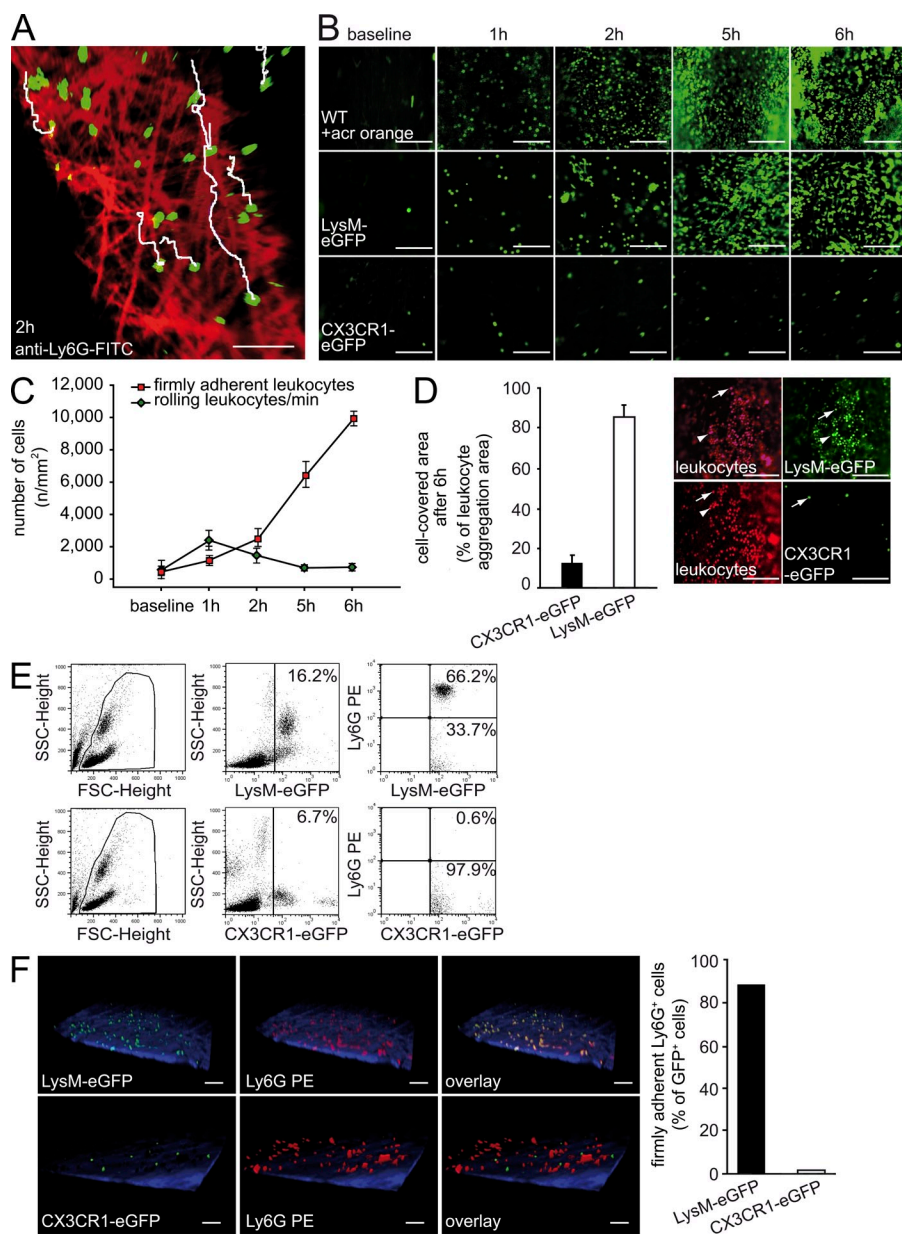
**Figure 3. Neutrophils and monocytes are the main leukocyte subsets accumulating during the initiation of DVT.** (A) Neutrophils (green) crawling on the vessel wall (red) of the IVC 2 h after DVT induction visualized by two-photon microscopy. Tracks of individual neutrophils are shown in white (also see Video 3). Bar, 50 µm. Shown is a representative of $n = 3$ experiments. (B) Time course of early leukocyte–endothelial interaction within 6 h of flow restriction as evaluated by intravital microscopy in WT animals using Acridine orange (WT + acr orange). Baseline images were taken before ligation. LysM-eGFP mice were used to evaluate neutrophils and CX₃CR1-eGFP mice were analyzed to evaluate monocytes. Bars, 100 µm. Shown is a representative of $n = 5$ experiments. (C) Dynamics of the recruitment of distinct subsets of innate immune cells during DVT initiation determined in vivo by video microscopy. Rolling and firm adhesion of leukocytes are given as number per square millimeter. Results are shown as mean ± SEM ($n = 5$ per group). (D, Left) Relative frequency of neutrophils and monocytes at 6 h of flow restriction as assessed by intravital video microscopy. Results are mean ± SEM ($n = 5$ per group). (D, Right) Representative images taken by intravital epifluorescence microscopy showing blood cell recruitment 6 h after flow restriction in the IVC. Neutrophils were visualized in LysM-eGFP mice. The number of recruited monocytes was assessed using CX3CR1-eGFP mice. In both strains of mice, all leukocytes (irrespective of their lineage) were identified by counterstaining with the fluorescent dye Acridine orange (pseudocolored in red). Bars, 100 µm. (E) FACS analysis of blood in LysM-eGFP and CX3CR1-eGFP mice without IVC ligation using a neutrophil specific anti-Ly6G antibody. (F) Intravital two-photon microscopy of LysM-eGFP and CX3CR1-eGFP with PE-labeled anti-Ly6G antibody 6 h after DVT induction (left). Bars, 50 µm. Quantification of Ly6G+ GFP+ double-positive cells in these mouse strains (right; Videos 4 and 5). Shown is a representative of $n = 3$ experiments.

leukocyte recruitment or thrombus formation (Fig. 4 F). Hence, predominantly endothelial P-selectin contributes to leukocyte recruitment and DVT formation in response to flow restriction, whereas platelet P-selectin appears to be less important.

Blood cell–derived TF is a central initiator of DVT

Next, we investigated how innate immune cells initiate DVT development. Activation of blood coagulation is likely to play a central role in our model, as enoxaparin efficiently prevented thrombus formation (Fig. 1 D). Because TF is the major initiator of coagulation and because different leukocytes express TF (Furie and Furie, 2007; Manly et al., 2011), we investigated the participation of blood cell–derived TF in DVT development. To examine the overall role of TF, we compared transgenic mice that express no mouse TF and only minimal (<1%) amounts of human TF (low-hTF) with mice expressing normal levels of human TF (HCV; Pawlinski et al., 2007). In HCV mice, flow restriction resulted in robust fibrin deposition within 6 h. In contrast, fibrin formation was completely abolished in low-hTF mice and DVT development was never observed (Fig. 5, A and B). Hence, TF-driven coagulation is indispensable for thrombus formation in response to flow restriction. Notably, loss of TF did not affect leukocyte recruitment, indicating that coagulation is not required to establish the inflammatory response during DVT (Fig. 5 C).
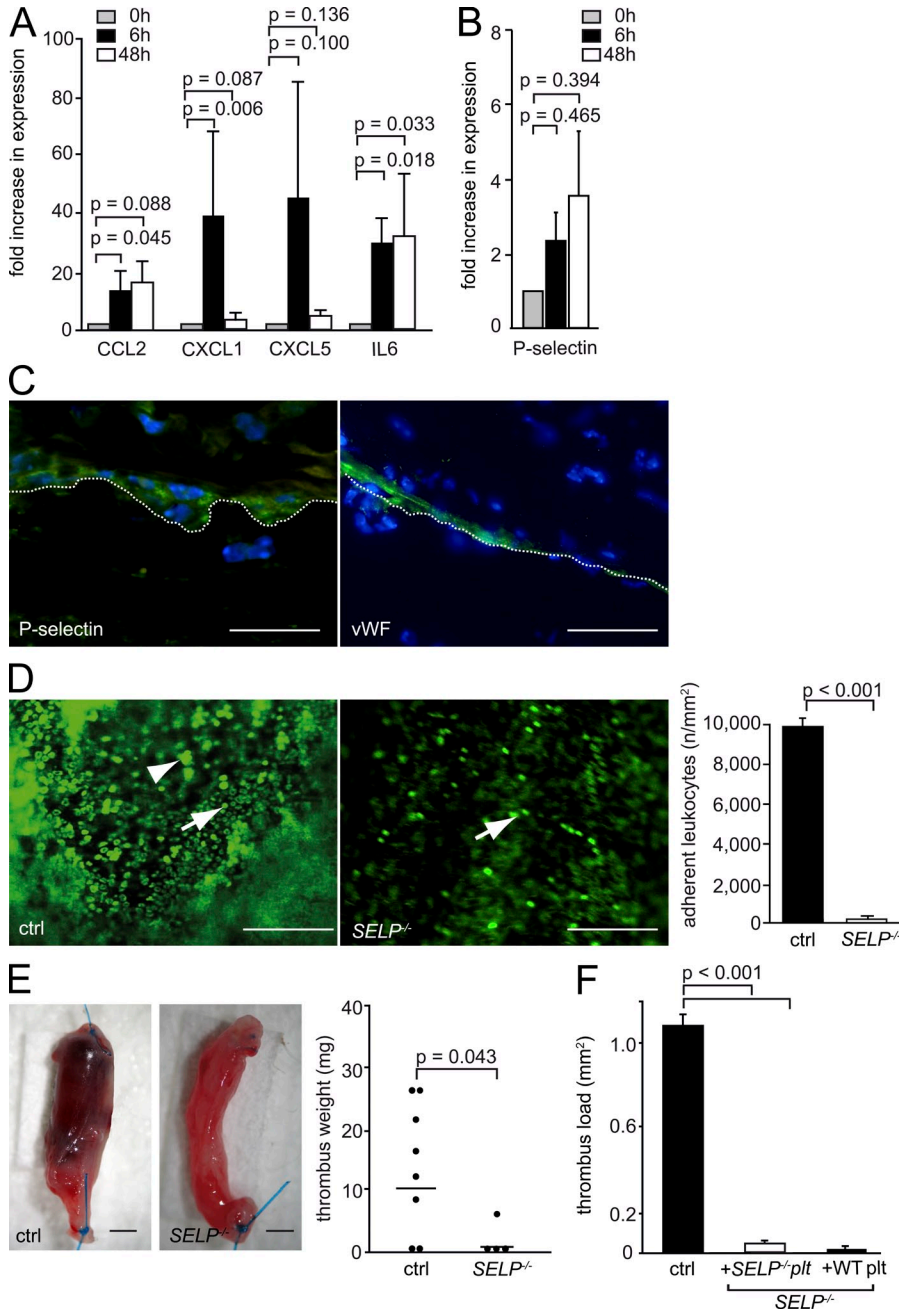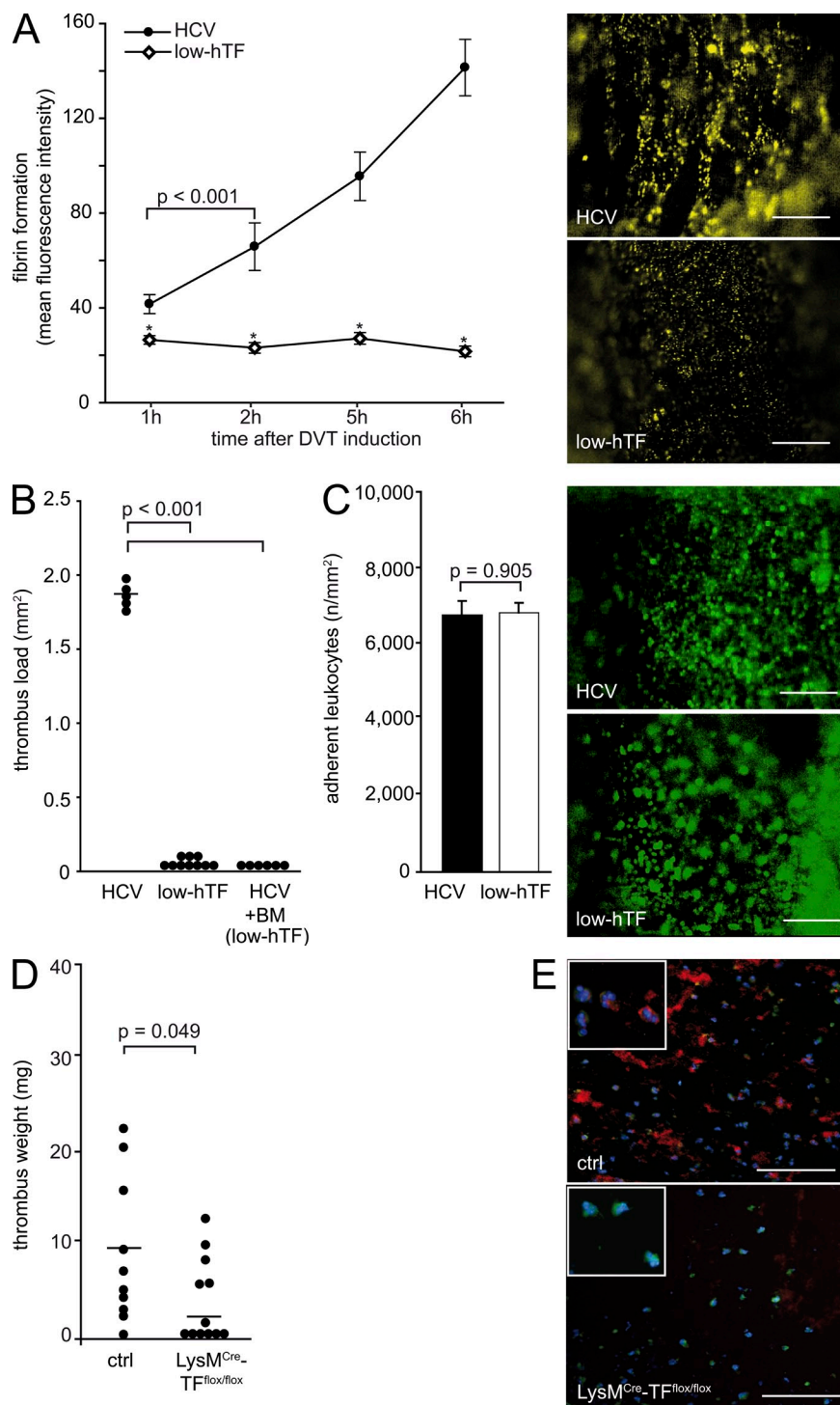
Figure 4. Crucial role of P-selectin for leukocyte accumulation in DVT. (A) RT-PCR of trafficking molecules in the IVC in response to flow restriction at baseline or 6 and 48 h after DVT induction ($n = 5$ per group). Results are shown as mean ± standard deviation. (B) RT-PCR of P-selectin in the IVC at baseline or 6 and 48 h after DVT induction ($n = 5$ per group). Results are shown as mean ± standard deviation. (C) Representative immunohistochemical stainings of the IVC endothelium 48 h after DVT induction showing P-selectin and vWF on the endothelial surface. Nuclei are counterstained with DAPI. Bars, 50 µm. (D, Left) Representative in vivo images of adherent leukocytes in C57BL/6 and $SELP^{-/-}$ mice 6 h after induction of DVT. Leukocytes were stained with Acridine orange and visualized by intravital video microscopy (arrowhead indicates aggregates; arrows indicate single adherent cells). Bars, 100 µm. (D, Right) Quantitative analysis of firm leukocyte adhesion, 6 h after flow restriction. Firm cell adhesion is given in number per square millimeters of C57BL/6 ($n = 5$) and $SELP^{-/-}$ ($n = 7$). Data are shown as mean ± SEM. (E, Left) Representative images of the excised IVC including the thrombus after 48 h in C57BL/6 and $SELP^{-/-}$ mice. Bars, 1 mm. (E, Right) Thrombus weight in C57BL/6 ($n = 8$) and $SELP^{-/-}$ mice ($n = 4$) 48 h after DVT induction. Dots represent individual experiments; lines show the mean of each group. (F) Histological analysis of the harvested IVC thrombi 48 h after flow reduction given as thrombus load in square millimeters ($n = 5$). plt, platelets. Data are shown as mean ± SEM.

formation was significantly attenuated compared with WT animals, confirming the major role of myeloid blood cell–derived TF for DVT development (Fig. 5 D). The procoagulant activity of myeloid cells isolated from LysM[Cre]–TF[flox/flox] mice is significantly reduced, yet not fully inhibited (Pawlinski et al., 2010). This is likely to explain the different degrees of protection from DVT observed in LysM[Cre]–TF[flox/flox] mice as compared with low-hTF chimeras. Predominantly, Ly6G^{−} monocytes and, to a lesser extent, Ly6G^{+} neutrophils expressed TF in venous thrombi (Fig. 5 E), suggesting that both subsets, particularly monocytes, contribute to TF-driven coagulation during mouse DVT.

Neutrophils promote propagation of DVT via NET formation

Given their frequency among leukocytes recruited to the IVC, we next examined the contribution of neutrophils to DVT development in more detail. To address this, we depleted neutrophils by injection of an anti–Ly6G antibody and

To define the source of TF and to differentiate whether TF expressed by blood cells or by the vessel wall contributes to DVT development, we next analyzed HCV mice that had been transplanted with low-hTF bone marrow cells. None of these chimeras developed DVT within 48 h of flow restriction (Fig. 5 B). This indicates that hematopoietic TF, but not vessel wall TF, is responsible for initiation of DVT in response to depressed venous blood flow without overt vessel damage. To specifically evaluate the participation of TF expressed by myeloid leukocytes, we analyzed mice with a deletion of TF in myeloid leukocytes (LysM[Cre]–TF[flox/flox] mice), including both monocytes and neutrophils (Pawlinski et al., 2010). In these mice, thrombus
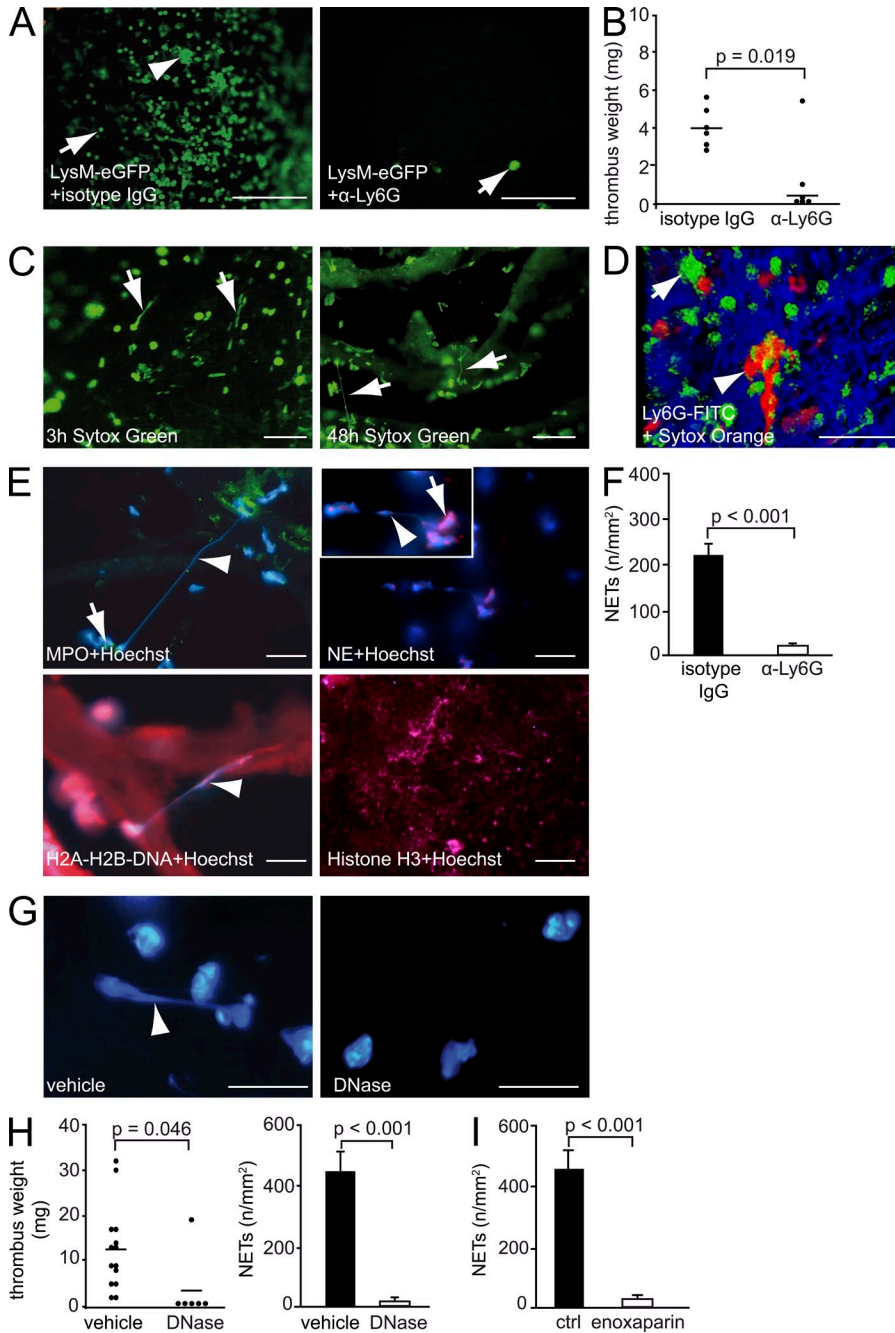
Figure 5. Blood cell TF is indispensable for venous thrombosis. (A) Fibrin formation during DVT development was measured in vivo by intravital microscopy in control HCV and low-hTF mice using an Alexa Fluor 488–labeled specific fibrin antibody. Measurements were performed after 1–6 h of flow restriction. Representative images acquired by intravital microscopy of the IVC are shown on the right (fibrin pseudo-colored in yellow). Bars, 100 μm. $n = 3$ per group. Data are shown as mean ± SEM. (B) Thrombus load was assessed on vG-stained serial sections in low-hTF ($n = 10$) and HCV mice ($n = 5$), as well as in bone marrow chimeras lacking blood cell TF ($n = 6$). Thrombus load is given as square millimeters. Dots represent individual experiments; lines show the mean of each group. (C) Assessment of leukocyte recruitment 6 h after flow reduction by intravital microscopy. Leukocytes were visualized using i.v. application of the fluorescent dye rhodamine 6G (pseudo-colored in green). The number of adherent cells is given as number per square millimeters ($n = 3$ per group). Representative in vivo images are shown on the right. Bar, 100 μm. Data are shown as mean ± SEM. (D) Thrombus weight (at 48 h) in control mice ($n = 10$) and in conditional mutants (LysM^{Cre}-TF$^{flox/flox}$) lacking TF in LysM$^+$ myeloid cells ($n = 12$). Dots represent individual experiments; lines show the mean of each group. (E) Immunohistochemical detection of TF protein (red) on Ly6G-positive (green) and -negative cells in thrombi at 48 h of flow restriction, indicating TF expression on neutrophils (yellow; TF$^+$ and Ly6G$^+$) and monocytes (red; TF$^+$ and Ly6G$^-$). LysM^{Cre}-TF$^{flox/flox}$ mice (bottom) were used as negative control. Nuclei are stained with DAPI. Bars, 100 μm. Shown is a representative of $n = 3$ experiments.

apart from acting as a potential source of myeloid TF, neutrophils deliver additional signals supporting venous thrombogenesis. Recently, activated neutrophils have been shown to release NETs, which consist of extracellular chromatin fibers with a backbone of histones (Brinkmann et al., 2004) and which may exert prothrombotic effects in vitro. Although release of NETs has been previously observed in a baboon model of venous thrombosis and in sepsis-induced microcirculatory thrombosis (Clark et al., 2007; Fuchs et al., 2010), the functional consequences of NETosis and their in vivo relevance for thrombogenesis in large veins remain unaddressed. Hence, we investigated here whether neutrophils might contribute to thrombus formation via release of NETs (Brinkmann et al., 2004). In fact, after 3 h of flow restriction, we found large amounts of intravascular extracellular DNA

induced flow restriction in the IVC (Fig. 6 A and not depicted). To our surprise, neutropenic mice developed no or significantly smaller thrombi compared with isotype-treated controls within 48 h of flow restriction (Fig. 6 B). This suggests that monocytes and monocyte-derived TF cannot fully compensate for a loss of neutrophils during DVT.

Because TF expression by Ly6G$^+$ neutrophils was weak compared with monocytes (Fig. 5 E), it seemed likely that,

Figure 6. NETs propagate DVT in vivo.
(A) Leukocyte accumulation in vivo at 6 h of flow restriction in the IVC of LysM-eGFP mice treated with control antibody or the anti-Ly6G mAb to deplete neutrophils. Arrowhead: aggregated neutrophils; arrows: single, adherent cells. Bars, 100 µm. (B) Thrombus weight 48 h after DVT induction in isotype and anti-Ly6G–treated WT mice ($n = 6$ per group). Dots represent individual experiments; lines show the mean of each group. (C) Representative image of $n = 3$ experiments of intravital microscopy 3 or 48 h after flow reduction showing Sytox Green+ NETs in the IVC. Bars, 50 µm. (D) Visualization of NETs in vivo by 2-photon microscopy. Ly6G-positive neutrophils (green, FITC anti-Ly6G antibody) attached to the vessel wall (blue) release Sytox orange–positive (red) NET structures inside the IVC 4 h after flow reduction (also see Video 7). Sytox orange–positive nuclei correspond to dying neutrophils, which have not (yet) exposed their DNA to the extracellular space. Arrowhead: extracellular DNA; arrow: neutrophil. Bar, 50 µm. (E) Immunohistochemical visualization of NETs by staining for DNA (Hoechst), MPO, NE, and histones (H2A-H2B-DNA, H3) in the IVC of WT mice 48 h after induction of DVT. Hoechst+ DNA originating from MPO+NE+ neutrophils (arrows) could be detected. Arrows, nuclei; arrowheads, NET fibers. Bars, 10 µm. (F) Number of NETs in neutropenic mice were quantified in thrombi after treatment with anti-Ly6G and isotype control antibody ($n = 3$ per group). Data are shown as mean ± SEM. (G) Representative images of WT thrombi stained with Hoechst after DNase1 treatment. Arrowhead, NET fiber. Bars, 10 µm. Shown is a representative of $n = 3$ experiments. (H) After injection of DNase1, thrombus weight (left) in the IVC was determined after 48 h of flow restriction. Dots represent individual experiments; lines show the mean of each group. Quantification of NETs is also shown (right) as mean ± SEM. Data were obtained in WT injected with normal saline i.v. ($n = 14$) or DNase1 ($n = 6$). (I) Quantification of NETs at 48 h in the enoxaparin-treated animals ($n = 4$ per group). Data are shown as mean ± SEM.

revealing a typical NET morphology (Fig. 6 C and Video 6). Intravital 2-PIVM revealed that extracellular DNA originates from Ly6G+ neutrophils (Fig. 6 D and Video 7). Extracellular DNA was located in close proximity to neutrophils and stained positive for the neutrophil granule proteins MPO, neutrophil elastase (NE), and the histone proteins H2A-H2B and H3, confirming that these structures were NETs (Fig. 6 E and not depicted). NETs were virtually absent in neutropenic mice, indicating that neutrophils are the major source of NETs during DVT development (Fig. 6 F).

Because platelets and a dense network of fibrin/fibrinogen surrounded the NETs, we analyzed in more detail whether NETs concentrate prothrombotic factors on their surfaces. In fact, the NETs were decorated with TF and protein disulfide isomerase, an enzyme implicated in the activation of blood cell–derived TF, supporting the concept that they might act as a prothrombotic surface (not depicted; Reinhardt et al., 2008). Hence, we next examined the functional relevance of NETs for DVT formation and treated mice with DNase1. Administration of DNase1 reduced NETs and at the same time significantly suppressed DVT growth (Fig. 6, G and H).
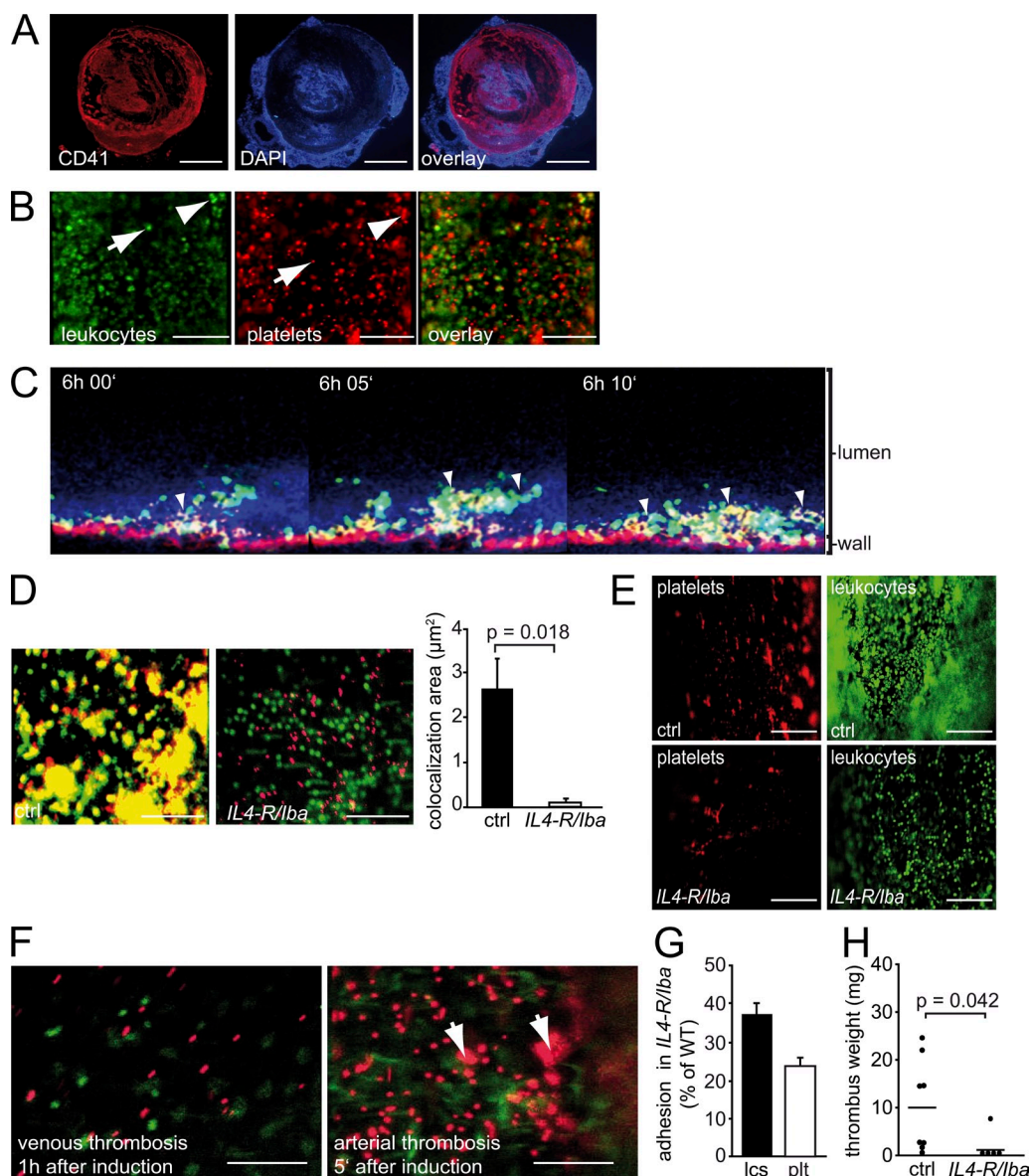
Figure 7. Platelet recruitment supports DVT formation in vivo. (A) Immunohistological cross sections of the IVC 48 h after DVT induction display platelet accumulation (CD41^{+}) within the thrombus. Nuclei are counterstained with DAPI. Bars, 200 µm. Representative of $n = 3$ experiments. (B) Representative images of intravital video microscopy of blood cell recruitment taken at 6 h after DVT induction. Arrowheads: thrombi; arrows: single, adherent cells. Platelets, red (rhodamine B); leukocytes, green (Acridine orange). Bars, 100 µm. (C) Time-lapse images of the developing thrombus (arrowheads) visualized by two-photon microscopy 6 h after DVT induction. Platelets (yellow) and neutrophils (green) are recruited from the bloodstream (blue) to the vessel wall (red; see also Video 8). (D) Platelet–leukocyte interaction was determined by intravital microscopy in C57BL/6 and *IL4-R/Iba* mice after 6 h of flow restriction. Bars: (left) 50 µm; (right) 100 µm. The right panel shows quantification of colocalization of leukocytes and platelets in WT ($n = 5$) and *IL4-R/Iba* mice ($n = 4$). Data are shown as mean ± SEM. (E) Representative images obtained by video microscopy 6 h after DVT induction in *IL4-R/Iba* and control animals ($n = 3$ per group). Platelets are pseudocolored in red (DyLight488-labeled GPIbβ antibody) and leukocytes in green (Acridine orange). Bars, 100 µm. (F) Representative images taken by intravital microscopy of WT mice 1 h after induction of venous (left) and 5 min after arterial (right) thrombosis. Arrows show platelet aggregate formation. Leukocytes are fluorescently labeled (green) by i.v. application of Acridine orange. Bars, 50 µm. (G) Quantitative analysis of platelet (plt) and leukocyte (lcs) accumulation (as percentage of WT controls) in *IL4-R/Iba* ($n = 3$) and WT mice ($n = 5$). Data are shown as mean ± SEM. (H) Thrombus weight at 48 h after DVT induction in C57BL/6 ($n = 8$) and *IL4-R/Iba* mice ($n = 5$). Dots represent individual experiments; lines show the mean of each group.

Together, these findings indicate that NETs are no innocent bystanders but rather contribute to neutrophil-driven coagulation during DVT propagation. Heparin, which has a high affinity for histones (Pal et al., 1983) and fosters degradation of NETs in vitro (Fuchs et al., 2010), reduced the formation of NETs during DVT in vivo (Fig. 6 I), an effect which might add to the antithrombotic actions of the drug.
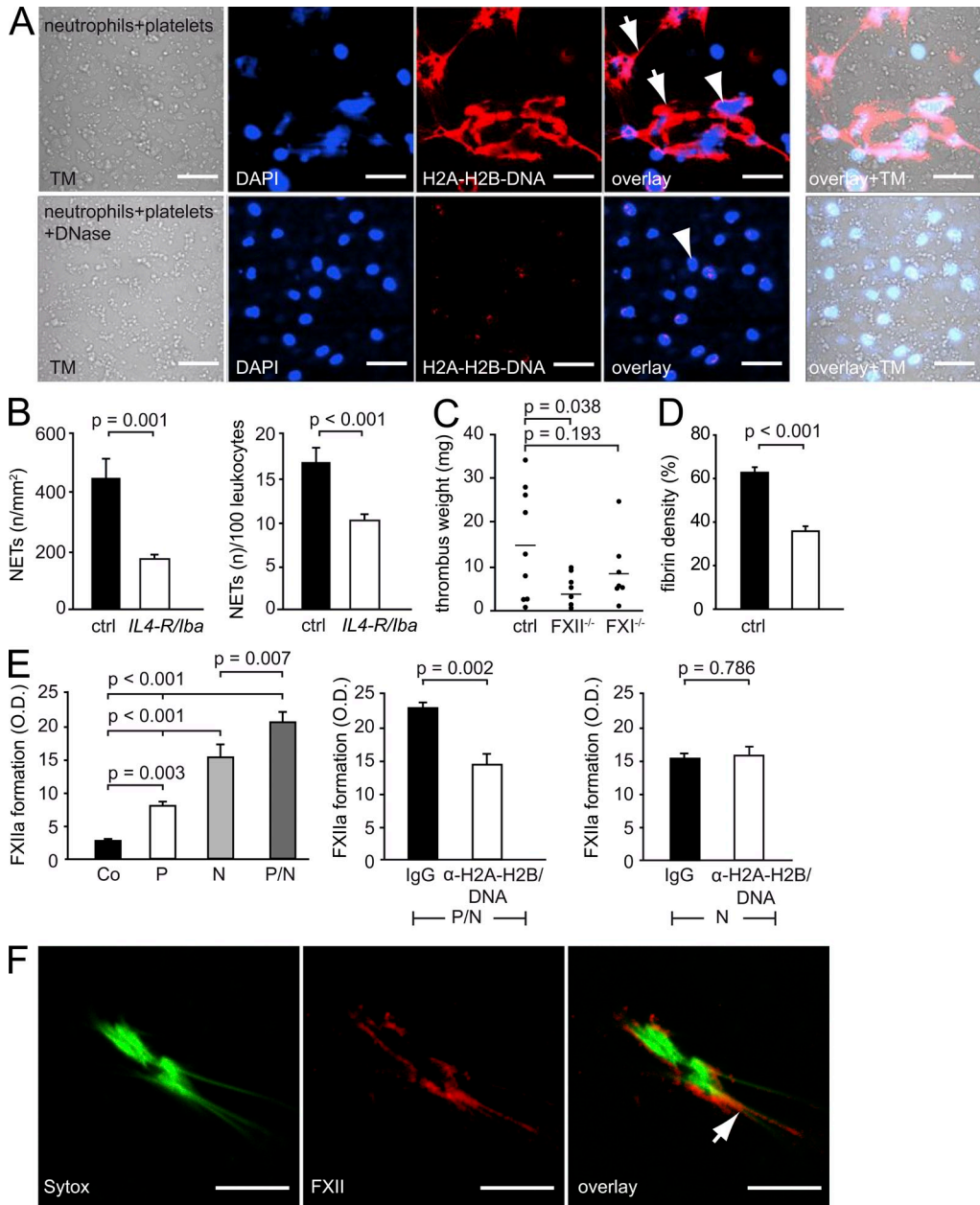
Figure 8. Platelets induce NET formation, which triggers FXIIa–dependent thrombus propagation. (A) Freshly isolated human neutrophils were incubated with platelet supernatant. Cells were stained with a primary antibody directed against DNA–histone complexes and DAPI and visualized by confocal microscopy. Incubation with DNase1 where indicated. Bars, 50 μm. Arrowheads, cell nucleus; arrows, NET. (B) The total number of NETs (left) and NETs per leukocyte (right) was quantified on cross sections of thrombi 48 h after flow restriction in *IL4-R/Iba* mice and WT animals ($n = 3$ per group). Data are shown as mean ± SEM. (C) Analysis of thrombus formation (milligrams) in the IVC of C57BL/6 ($n = 9$), FXII$^{-/-}$ deficient ($n = 7$), and FXI$^{-/-}$ deficient mice ($n = 7$) 48 h after flow reduction. Dots represent individual experiments; lines show the mean of each group. (D) Quantification of fibrin density as percentage of fibrin-covered area in the IVC thrombus ($n = 4$ per group). Data are shown as mean ± SEM. (E) The effects of co-incubation of activated platelets (P) and neutrophils (N) on FXII activation in vitro. NETosis was inhibited by an antibody directed against the H2A–H2B–DNA complex. Data are shown as mean ± SEM. (F) Confocal visualization of FXII on NETs, released from isolated human neutrophils. Arrow, FXII bound to Sytox Green$^+$ NETs. Bars, 10 μm.

Platelets support DVT formation

In addition to leukocytes, platelets are recruited during DVT formation (Fig. 7 A). Intravital microscopy indicated that platelet adhesion occurred within 2 h of flow restriction and increased over time (not depicted and Fig. 7 B). After 6 h, 2P-IVM revealed that most platelets adhered either directly to the intact endothelium or were attached to adherent leukocytes (Fig. 7 C and Videos 8–10). Platelets and leukocytes formed heterotypic aggregates (Fig. 7, B–D). Considering that only 10% of the circulating platelets are labeled in our

model, we estimated that on average each adherent leukocyte carries at least one platelet (Fig. 7, B–D). Platelet–leukocyte interactions depended on the platelet vWF-receptor glyco-protein (GP) Ibα. Correspondingly, the interaction of plate-lets and leukocytes was virtually abrogated in *IL4-R/Iba* mice, lacking the external GPIbα domain (Fig. 7 D).

To evaluate the quantitative contribution of platelets to the cellular content of the thrombus, we stained 100% of platelets by injecting a fluorescently labeled anti–GPIbβ anti-body, which does not interfere with platelet adhesion and aggregation. After 6 h of flow reduction, platelets were dif-fusely distributed as individual cells across the thrombus and formed small aggregates. However, the number of recruited leukocytes clearly outnumbered platelet accumulation (Fig. 7 E). In contrast to arterial thrombosis, where platelets accumulate within minutes and form large aggregates (Massberg et al., 2010), platelets were mainly recruited as individual cells after several hours in venous thrombosis and formed only very few small aggregates (Fig. 7, E and F). This suggests that homo-typic platelet aggregation does not play a crucial role for the initiation of venous thrombus formation.

The platelet vWF receptor GPIbα was important for overall platelet recruitment and DVT progression, as both were markedly reduced in *IL4-R/Iba* mice (Fig. 7, G and H; and not depicted). Likewise, venous thrombus formation was significantly reduced in platelet-depleted mice (by 95% compared with controls, $n = 6$–8; P < 0.001).

Because GPIb-dependent platelet–leukocyte interactions were a prominent phenomenon in venous thrombi (Fig. 7, B–D), we addressed whether platelets support DVT develop-ment by fostering neutrophil-dependent coagulation. In fact, leukocyte accumulation was markedly decreased in *IL4-R/Iba* mice (Fig. 7, E and G), suggesting that platelets promote leukocyte recruitment. In addition, platelets also supported NETosis as NETs were rapidly released from neutrophils when we incubated them with activated platelets in vitro (Massberg et al., 2010; Fig. 8 A). This was confirmed by our in vivo experiments, as the number of NETs released per re-cruited leukocyte was significantly attenuated in *IL4-R/Iba* mice (Fig. 8 B). Hence, the GPIbα–dependent interaction of platelets with leukocytes exerts a dual function during DVT development: (1) it supports leukocyte recruitment; and (2) it stimulates NET formation by neutrophils.

Neutrophils amplify DVT by initiating FXII–dependent coagulation

Finally, we asked how the interplay of platelets and netting neutrophils might contribute to venous thrombogenesis, which is critically dependent on activation of the coagulation system. Negatively charged surfaces can trigger activation of FXII, the initiator of the intrinsic coagulation pathway. Because NETs are negatively charged, we hypothesized that NETs could potentially activate FXII during DVT (e.g., via their polyanionic DNA components). In fact, we found that thrombus formation is significantly reduced after injection of the FXII inhibitor PCK (not depicted) or in mice lacking

FXII (Fig. 8 C). In contrast, thrombus weight was only mod-erately (nonsignificantly) reduced in FXI-deficient mice, in-dicating that the ability of FXIIa to propagate DVT is largely independent of FXI activation. As FXIIa can enhance the density of fibrin networks without stimulating thrombin generation via FXIa (Konings et al., 2011), we measured the density of fibrin deposition in thrombi of FXII-deficient mice. The percentage of fibrin–covered area in thrombi of FXII-deficient mice was decreased compared with WT (Fig. 8 D), suggesting that FXIIa might indeed amplify DVT by inter-acting directly with fibrin.

To further substantiate this concept, we examined in vitro whether FXII is activated in response to platelet-dependent NET formation. Activated neutrophils alone were able to trigger FXII activation (Fig. 8 E, left). This did not involve NETs because it remained unaffected by the anti–H2A-H2B antibody (Fig. 8 E, right). In the presence of activated plate-lets, the capacity of neutrophils to trigger FXII activation was significantly increased, suggesting an additive effect of neutrophils and platelets (Fig. 8 E, left). The anti–H2A-H2B antibody completely abolished the effect of platelets on FXIIa formation by neutrophils, suggesting that platelet-driven aug-mentation of neutrophil FXIIa formation requires the pres-ence of NETs (Fig. 8 E, middle). When we analyzed NETs by confocal microscopy, we found that they were decorated with FXII (Fig. 8 F). Collectively, these findings suggest that NETs are able to bind FXII on their surfaces and provide a scaffold for FXII activation, presumably by facilitating auto-activation of FXII via their negatively charged extracellular DNA surfaces. Hence, NET-driven FXII activation is of major relevance for propagation of intravascular thrombus formation during DVT.

DISCUSSION

The sequence of events that trigger large vein thrombosis in response to stasis has remained poorly defined. Using a novel mouse model of flow restriction–induced DVT, we have un-covered the mechanisms underlying the previously proposed link between thrombosis and inflammation crucial for the pathogenesis of DVT. By two-photon microscopy, we show that flow restriction triggers the rapid accumulation of neu-trophils and monocytes, which is indispensable for DVT development. Innate immune cells initiate local fibrin forma-tion predominantly through delivery of TF. In addition, neutrophils form NETs, triggering FXII-dependent coagula-tion. Although TF appears to be required to initiate DVT, neutrophil-driven coagulation contributes to DVT propaga-tion. Platelets foster leukocyte accumulation and support fibrin formation by enhancing neutrophil-dependent coagulation. Hence, by combining a novel DVT model with in vivo imag-ing we have uncovered different processes responsible for the emergence of localized thrombosis in response to reduced venous blood flow, an important trigger of DVT in humans.

The cellular events initiating DVT during compromised venous blood flow remained unclear, mostly as a result of the lack of an appropriate rodent model. Previous studies

performed in mice predominantly used endothelial injury to induce DVT (Eitzman et al., 2000; Angelillo-Scherrer et al., 2001; Wang et al., 2006). However, exposure of subendothelial matrix is a rare cause of DVT in humans (Sevitt, 1974; Mackman, 2008), suggesting that findings obtained from models that use endothelial disruption as a thrombogenic stimulus may have limited relevance for the clinical setting (Sevitt, 1974; Mackman, 2008). Here, we therefore established a novel mouse model in which venous thrombosis is initiated by depression of venous blood flow in the absence of endothelial disruption. Several aspects indicate that our model closely resembles DVT formation in humans. First, perturbation, but not complete cessation, of venous blood flow is a common trigger, though not the only trigger of DVT formation in patients. Second, similar to the time course in humans (Warlow et al., 1976), DVT developed over a prolonged period of time (12–48 h). Third, the layered multicellular structure of the thrombi is reminiscent of human venous thrombi (Sevitt, 1974). Fourth, enoxaparin, the standard prophylactic strategy in human patients, also prevented venous thrombosis in our model. Although our approach does not account for other triggers of venous thrombogenesis, including malignancies, sepsis, or hereditary disorders, the DVT model presented here will be valuable for evaluation of new drugs implicated in prophylaxis and treatment of DVT in the large group of human patients, in which compromised venous blood flow is the major mechanism of DVT formation.

By combining this novel model with state-of-the-art intravital imaging, we defined the subsets of blood cells recruited to the vessel wall within the first hours of depressed venous blood flow. We observed that P-selectin–dependent neutrophil and monocyte recruitment is critical for DVT formation. Although the exact triggers of P-selectin exposure remain unclear, hypoxia and changes in shear forces are likely mechanisms. Recently, soluble P-selectin has been established as a diagnostic marker for DVT, supporting a clinical role of this adhesion molecule (Ramacciotti et al., 2011). In addition, several chemokines were up-regulated in the venous vessel wall in response to flow restriction. Together, this supports a critical role of sterile inflammation in venous thrombogenesis, consistent with the clinical observation of increased levels of inflammatory biomarkers, such as CRP, in human DVT patients (Bucek et al., 2002).

But how do innate immune cells trigger DVT? In view of the extensive intravascular fibrin formation typical for DVT, it is generally assumed that the coagulation system plays a critical role for venous thrombosis. Nevertheless, the mechanisms that drive fibrin formation remained largely unclear. We have identified innate immune cells as the primary initiators of clot formation contributing to DVT by two distinct mechanisms: (1) through delivery of TF; and (2) by release of procoagulant NETs.

Earlier studies applying endothelial disruption or complete IVC occlusion suggested that thrombus formation in the venous vasculature is primarily driven by TF from the vessel wall (Day et al., 2005; Zhou et al., 2009). Here, we report that blood cell–derived TF, and not vessel wall TF, critically contributes to venous thrombosis, which could be explained by two factors: (1) we did not completely abrogate venous blood flow allowing a continuous accumulation of leukocytes during DVT initiation; and (2) endothelial denudation was absent in our model, limiting the contribution of vessel wall–derived TF. Mice lacking TF in the myeloid blood cell lineage were protected from DVT development, demonstrating that blood cell TF is mainly delivered by this cell type. Because LysM is active in both neutrophils and monocyte subsets, the LysM^{Cre}–TF$^{flox/flox}$ strain used in our experiments does not allow differentiation of the relative contribution of neutrophil or monocytes to the local delivery of blood cell–derived TF. However, two of our findings favor monocytes as a major source of TF in our DVT model: (1) we found that TF expression by Ly6G$^+$ neutrophils was weak, whereas monocytes revealed a strong TF signal; and (2) we observed that neutrophils contribute to DVT in a process involving NET formation and FXII activation and that inhibition of these pathways significantly attenuates DVT formation. This suggests that NET formation and FXII activation, rather than delivery of TF, are the predominant neutrophil–dependent contributions to thrombogenesis in our DVT model. Nevertheless, we cannot rule out that neutrophil-derived TF also contributes to DVT progression in this model.

Consistent with other models, we observed that neutrophils constitute the predominant leukocyte subset recruited to the site of DVT (Stewart et al., 1974; Zhou et al., 2009; Diaz et al., 2010). Although neutrophils have previously been involved in postthrombotic remodeling of the vein wall (Varma et al., 2003), their contribution to venous thrombus formation has remained unclear. Here, we show that neutrophil depletion results in a profound inhibition of DVT development. Neutrophils recruited to the IVC wall generate NETs, which are known to act as prothrombotic scaffolds by binding vWF, degrading potent anticoagulants like TF pathway inhibitor, and reducing thrombomodulin-dependent protein C activation (Ward et al., 1997; Fuchs et al., 2010; Massberg et al., 2010; Ammollo et al., 2011). Although NETs have been found in baboon DVT (Fuchs et al., 2010), their functional significance for venous thrombogenesis remained unclear. Here, we report that inhibition of NETosis resulted in an attenuated DVT progression. We show that activated platelets bind to neutrophils in a process involving GPIb. This interaction fosters NET formation, as has been reported by others previously (Clark et al., 2007). NETs, in turn, act as a procoagulant surface propagating DVT development through the binding and activation of FXII. Hence, our present study provides direct in vivo evidence that NETs represent an important mechanistic link between neutrophil-driven venous inflammation and venous thrombogenesis. Interestingly, generation of NETs has recently been reported in disease states known to be linked with an increased risk of thrombotic disorders, such as systemic lupus erythematosus (Garcia-Romo et al., 2011). However, future studies will have to address

whether neutrophils and NETs also contribute to DVT in settings where venous stasis is not the primary trigger of thrombogenesis, e.g., in cancer or sepsis patients.

Because negatively charged surfaces (as the ones provided by NETs) are a major trigger of FXII activation (Griep et al., 1985), we evaluated here whether activation of the contact pathway might contribute to the prothrombotic actions of NETs. In fact, we found that NETs bind and activate FXII in vitro. In addition, inhibition or genetic ablation of FXII provided protection against DVT propagation, suggesting that FXIIa contributes to the prothrombotic potential of NETs. Consistent with previous observations in arterial thrombosis (Cheng et al., 2010), FXI deficiency only had a minor impact on venous thrombogenesis. This indicates that FXIIa contributes to venous thrombogenesis predominantly using FXI–independent pathways, e.g., via a direct stabilization of the fibrin network (Konings et al., 2011).

Together, our study identifies NETs as a platform of thrombogenesis in large veins in response to perturbation of flow. We observed that mice deficient in blood cell TF have no thrombi, whereas neutropenia or loss of FXII results in a decreased thrombus weight but does not fully protect from DVT formation. This suggests that blood cell TF is required to initiate DVT, whereas neutrophil-driven coagulation, including activation of FXII, contributes to DVT propagation and stabilization in settings of compromised venous blood flow.

One of the most intriguing findings reported here is that platelets, the major players of arterial thrombosis, also contribute to the propagation of DVT in the absence of endothelial disruption. In fact, we found that platelets are recruited to developing venous thrombi early after flow restriction and contribute to DVT formation by supporting accumulation of innate immune cells and by binding to leukocytes, a process which initiates NET formation both in vitro and in vivo. GPIbα was essential for platelet-driven propagation of DVT, as it was required for both platelet accumulation in the thrombus and, particularly, for platelet–leukocyte interactions, which in turn augment the ability of neutrophils to release procoagulant NETs. Hence, platelets induce sterile inflammation and foster venous clot formation by cooperating with netting neutrophils. The critical role of platelets in DVT formation is further supported by the importance of vWF in DVT and by the clinical observation that the anti-platelet drug aspirin is prophylactic against venous thrombosis in high-risk patients undergoing orthopedic surgery, a condition frequently associated with compromised venous blood flow (PEP-Group, 2000; Brill et al., 2011). It should be mentioned, though, that the contribution of platelets to DVT might be different in settings where stasis is not the primary trigger.

In conclusion, our study shows that DVT in response to perturbed blood flow is driven by a concerted interaction of monocytes, netting neutrophils, and platelets and thus uncovers the mechanisms linking inflammation and venous thrombosis. Disruption of this cooperation and prevention of monocyte- and neutrophil-driven thrombogenesis paves the way for the development of novel therapeutic approaches, specifically targeting the cellular factors that initiate DVT development. Such a strategy might improve the benefit-to-risk profile of anticoagulant therapy in comparison with nonspecific inhibition of the final common coagulation pathway that is characteristic of current therapies.

MATERIALS AND METHODS

Animals. Specific pathogen-free WT C57BL/6J, SV129S1, and B6.129s7-Selp/J mice were obtained from Charles River. IL4Rα/GPIbα-tg (IL4-R/Iba) mice were generated as previously described (Kanaji et al., 2002). For intravital visualization, heterozygous CX3CR1[eGFP/+] and LysM[eGFP/+] knockin mice were used (Faust et al., 2000; Jung et al., 2000). CX3CR1[eGFP/+] mice were provided by S. Jung (Weizmann Institute of Science, Department of Immunology, Rehovot, Israel). LysM[eGFP/+] knockin mice were provided by T. Graf (Center of Genomic Regulation, Barcelona, Spain). HCV, Low-hTF, LysM[Cre], and TF[flox/flox] mice were maintained on the C57BL/6J background (Parry et al., 1998; Clausen et al., 1999; Pawlinski et al., 2007). LysM[Cre]-TF^{fl/fl} animals were generated by crossing LysM[Cre] with TF[flox/flox] mice as previously described (Pawlinski et al., 2010). FXII- and FXI-deficient mice were generated as previously described (Gailani et al., 1997; Pauer et al., 2004) and provided by J. Heesemann (Max von Pettenkofer-Insitut, Klinikum Innenstadt, Ludwig-Maximilians-Universität München, Munich, Germany). All mice used in the experiments were 8–14 wk old and weight and sex matched. All procedures performed on mice were approved by the local legislation on protection of animals (Regierung von Oberbayern, Munich) and the Immune Disease Institute's Animal Care and Use Committee (IDI 4M0109/HMS04564).

Mouse model of flow restriction in the IVC. Mice were anesthetized by intraperitoneal injection as described previously (Massberg et al., 2002). A median laparotomy was performed and the IVC was exposed by atraumatic surgery. We positioned a space holder (FloppyR II Guide Wire 0.014 in [0.36 mm]; Guidant Corporation) on the outside of the vessel and we placed a permanent narrowing ligature (8.0 monofil polypropylene filament, Premilene; Braun) exactly below the left renal vein. Subsequently, the wire was removed to avoid complete vessel occlusion. Side branches were not ligated or manipulated. Flow velocity was determined immediately after the flow restriction (Cap-Image 7.1). Because we wanted to rule out endothelial injury as a trigger for venous thrombosis, all mice with bleedings or any injury of the IVC during surgery were excluded from further analysis. There was no difference in the exclusion rate across the different experimental groups. After the procedure, a subset of animals was investigated by intravital microscopy. In the remainder, the median laparotomy was immediately sutured by a 7.0 polypropylene suture (Ethicon). For weight measurement, the vessel was excised just below the renal veins and proximal to the confluence of the common iliac veins. After the restriction procedure the blood flow velocity was reduced by ∼80% (Fig. 1 B). The shear stress was 0.144 dyne/cm² ± 0.02 SEM before the flow restriction and 0.072 dyne/cm² ± 0.017 SEM after the procedure in the IVC close to the site of ligation. Sham experiments consisted of preparation of the IVC and placement of the filament under the vessel without ligation.

In vivo model of arterial thrombosis by carotid artery ligation. As a model of arterial thrombosis, carotid injury was induced as previously described (Massberg et al., 2010).

Preparation of platelets and leukocytes for intravital microscopy. Murine platelets were isolated from whole blood and labeled with 5-carboxy-flourescein diacetate succinimidyl ester (DCF) or cell tracker violet (Invitrogen) as reported earlier (Massberg et al., 2002). The DCF-labeled platelet suspension was adjusted to a final concentration of 150×10^6 platelets/250 µl and injected i.v. via a jugular vein catheter. For in vivo staining, a nonblocking GPIbβ-binding fluorescent-labeled antibody (3 µg/animal; rat anti–mouse DyLight488-labeled GPIbβ antibody; Emfret Analytics) was infused i.v. Adhesion and aggregation of murine platelets were assessed by in vivo

video microscopy. For the qualification and quantification of leukocyte adhesion, rhodamine 6G (Invitrogen) or Acridine orange (Sigma-Aldrich) was injected i.v. to stain circulating leukocytes in vivo. To characterize platelet-leukocyte interactions in vivo, Acridine orange–stained leukocytes and ex vivo labeled platelets (20 µg/ml rhodamine B; Sigma-Aldrich) were imaged simultaneously. To differentiate neutrophils and monocytes, LysM-eGFP and CX3CR1-eGFP mice were used. The ratio of these cell types in relation to the total number of recruited leukocytes was analyzed by first taking images of the eGFP-labeled cells, followed by injection of Acridine orange to visualize all leukocytes. Detection of extracellular DNA (NET formation) in vivo was achieved by i.v. infusion of Sytox green or orange after flow reduction (1 µmol per animal).

Assessment of fibrin formation in vivo. Fibrin formation in vivo was measured in HCV and Low-hTF using an Alexa Flour 488 (Invitrogen) ex vivo labeled anti-fibrin antibody (2 mg/kg body weight, mouse anti-fibrin IIβ chain Bβ 15–42, clone T2G1; Accurate Chemical) which was injected i.v. This antibody specifically binds to fibrin formed in the vascular system. Fluorescence intensity was quantified by intravital video microscopy (BX51WI; Olympus). Fibrin formation is presented as mean fluorescence intensity (arbitrary units).

Intravital epifluorescence microscopy. The mice were anesthetized as described, the flow restricting procedure was performed, and the animals were fixed on a custom built-stage to maintain a physiological temperature. Measurements were performed with a high-speed wide-field Olympus BX51WI fluorescence microscope using a long-distance condenser and a 20× (NA 0.95) water immersion objective with a monochromator (MT 20; Olympus) and a charge-coupled device camera (ORCA-ER; Hamamatsu Photonics). For image acquisition and analysis a computer (Dell) with Cell^R (Olympus) software was used. Cell recruitment was quantified in four fields of view (50 × 100 µm) per animal; immotile cells were counted as adherent and moving cells were counted as rolling within 30 s as previously described (Massberg et al., 1998). The cell covered area (in square millimeters) and colocalization area was determined by planimetric measurement (Cap-Image 7.1).

Two-photon in vivo microscopy. For intravital imaging of the IVC in vivo, the TrimScope (LaVision Biotech) connected to an upright microscope (Olympus) was used, equipped with a MaiTai laser (Spectra-Physics) and a 20× 0.95 NA water immersion objective (Olympus). Pictures were acquired at 800 nm excitation wavelength in a 500 × 500-µm frame with 512 × 512 pixels and a z-step of 3 µm and detected by PMTs (G6780-20, Hamamatsu). ImSpector (LaVision Biotech) was used as acquisition software. The mice were anesthetized as described, the flow restricting procedure was performed, and the animals were fixed on a custom-built stage to maintain a physiological temperature. LysM-eGFP mice, CX3CR1-eGFP mice, and an FITC- or PE-labeled anti-Ly6G antibody (10 µg/animal; Clone 1A8; eBioscience) were used to visualize neutrophils and monocytes. In addition, cell tracker violet (Invitrogen)–labeled platelets and 2 MD TRITC-Dextran (Invitrogen) for visualization of the blood flow were infused. 3D reconstruction and volume rendering was done with by Volocity (PerkinElmer) and cell tracking with ImageJ software (National Institutes of Health).

Bone marrow transplantation. For generation of bone marrow chimeras, 3 × 10⁶ bone marrow cells of Low-hTF mice were injected into the tail vein of irradiated (900 rad) HCV (hTF) mice. 6 wk after transplantation, when a stable chimerism is guaranteed, thrombus formation was induced in the IVC and intravital video microscopy was performed (as described in the previous sections).

Inhibition of NETosis and depletion of neutrophils and platelets in vivo. DNase1 (100 U DNase1, RNase-free; Fermentas) was given i.v. 30 min before and 24 h after IVC ligation by tail vein injection, and normal saline injection served as control. Neutrophils were depleted by an anti-Ly6G antibody (5 mg/kg body weight; rat anti-mouse Ly6G, Clone 1A8; eBioscience) given i.v. 24 h before induction of thrombosis. The absence of neutrophils

was confirmed by a white blood cell count (Sysmex) of EDTA whole blood and by intravital video microscopy using LysM-eGFP mice. Platelet depletion was induced using the rat anti–mouse GPIbα (CD42b) antibody i.v. (2 mg/kg body weight; Emfret Analytics).

FXII inhibitor and enoxaparin treatment. C57BL/6J mice were treated with FXII inhibitor (H-D-Pro-Phe-Arg-chloromethylketone; 10 mg/kg body weight i.v.; Bachem) directly before stasis and then every 24 h. Enoxaparin was administered s.c. 3 h before and every 6 h after ligation in a dosage of 60 mg/kg body weight and FXa was monitored.

Histology. The IVC was excised, formalin fixed, and paraffin embedded. Serial cross sections or longitudinal sections of the ligated IVC were cut (2 µm) 6 and 48 h after flow reduction. Tissue sections were stained with HE, van Gieson's elastica stain, and MSB (Martius scarlet blue). Images were acquired using an epifluorescence microscope (DMRB; Leica) with an AxioCam (Carl Zeiss) and processed by AxioVision 4.6 software (Carl Zeiss). Where indicated, the thrombus load, a parameter which like the thrombus weight accounts for the size of the thrombus, was measured on serial cross sections by circling the outer edge of the luminal thrombus tissue in sections from the proximal, middle, and distal part of the IVC (Cap-Image 7.1). For Carstairs staining, slides were hydrated in xylol and ethanol to distilled water, followed by incubation in 5% ferric ammonium sulfate for 5 min and staining by Mayer hematoxylin for 5 min and Picric Acid-orange G solution for 45 min. After washing, slides were stained by Ponceau Fuchsin solution for 3 min, 1% phosphotungstic acid for 3–5 min, Anilin blue solution for 10 min, and rinsed in distilled water. Slides were dehydrated covered with a coverslip using mounting medium (Pertex). All reagents were provided by EMS. Fibrin density was quantified by ImageJ as the fibrin-positive area of the total thrombus area (percentage). Lungs were excised 48 h after DVT induction, formalin fixed, and paraffin embedded. Sections of 3 µm thickness were cut systematically of the whole lung to screen for signs of pulmonary embolism in HE staining.

Immunofluorescence stainings of frozen sections. For immunofluorescence staining of frozen sections, the excised vessel was immediately rinsed with PBS, embedded in OCT, and frozen at −80°C. The IVC was cut with a cryotome into sections of 5 µm thickness. Specimens were fixed with 4% formalin for 4 min, washed in PBS, and blocked with 5 µg/ml anti–mouse CD16/32 (eBioscience) and 1% BSA (PAA Laboratories) in PBS for 30 min. The sections were incubated with primary antibodies (Table S1) for 1 h at room temperature and washed in PBS + 0.1% Tween. Next, secondary antibodies (Table S1) were used for detection. For double staining, a sequential protocol was performed. DNA was stained with 1 µg/ml Hoechst 33342 (Invitrogen) or 1 µg/ml DAPI (Roth), and a coverslip was placed by mounting medium (DAKO). Images were acquired using an epifluorescence microscope (DMRB) with an AxioCam and processed by AxioVision 4.6 software or a two-photon microscope (TrimScope) and Volocity (Perkin-Elmer) as indicated. For quantification of NETs, serial cross sections were stained with Hoechst and the number of NETs was counted with a 40× objective in four fields of view (176 × 131 µm). The sections originated from the proximal, middle, and distal part of the IVC. For quantification of NET formation, three distinct parameters had to be met in our experiments: (1) presence of extracellular DNA protrusions; (2) the protrusion had to originate from cells staining positive for neutrophil markers; and (3) the structures had to be decorated with markers of neutrophil granule proteins including NE or MPO. Only if all of these criteria were fulfilled was a structure defined as NET and included into the quantification.

Computed tomography. Anaesthetized mice were imaged with the Inveon small animal PET/CT scanner (Siemens). Mice were kept fully sedated with 1.5% isoflurane during injections and imaging. To obtain vascular contrast, 0.1 ml of iodinated intravascular contrast agent eXIA 160-XL (Binitio Biomedical Inc.) was injected i.v. CT acquisition consisted of 270 projections acquired with exposure time of 400 ms, x-ray voltage of 80 kVp, and

anode current of 400 µA for a full 360° rotation. CT images were reconstructed using a modified Feldkamp algorithm. The resulting matrix was 256 × 256 pixels with 384 transverse slices (pixel size 0.17 × 0.17 × 0.17 mm).

Scanning and transmission electron microscopy. Mice were sacrificed and the IVC was perfused with 3 ml PBS (37°C) in C57BL/6, followed by perfusion fixation with 1% phosphate-buffered glutaraldehyde. The vein was carefully dissected and cut open longitudinally, further fixed by immersion in 1% PBS-buffered glutaraldehyde for 12 h, dehydrated in ethanol, and processed by critical point drying with CO_2. Thereafter, the veins were oriented with the lumen exposed, mounted with carbon paint, sputter coated with platinum, and examined using a field emission scanning electron microscope (JSM-6300F; Jeol Ltd; Massberg et al., 2003). The transmission electron microscopy was performed to characterize the ultrastructure of the venous vessel wall and the generated venous thrombi. The IVC of C57BL/6 mice was perfused with 3 ml PBS (37°C) and perfusion fixed in a solution consisting of 2.5% buffered glutaraldehyde and 2% paraformaldehyde in phosphate buffer, pH 7.4, overnight at 4°C. The specimens were mounted in epon solution and sections of 50–100 nm were prepared with an ultra microtome.

Confocal microscopy of NETs in vitro. For preparation of human neutrophils, blood was drawn from healthy donors into syringes containing Trinatrium citrat (1:10). Whole blood was added to dextran 3% (MW 500,000; 2:1) and inverted before red blood cells were allowed to separate for 30 min at room temperature. Thereafter, the supernatant was removed, layered on top of Ficoll (1:1), and centrifuged for 30 min at room temperature at 1,200 rpm. The supernatant was removed and the pellet was resuspended in RPMI/10 mM Hepes. Cells were centrifuged for 10 min at room temperature at 1,000 rpm. To lyse residual blood cells, the pellet was resuspended in 1 ml pyrogen-free water (ultrapure) and, after addition of RPMI/10 mM Hepes, centrifuged for 10 min at room temperature at 1,000 rpm. The pellet was resuspended in RPMI/10 mM Hepes.

Preparation of platelet supernatant. Platelets were isolated as described elsewhere (Massberg et al., 2010). 10^9 platelets were activated with 8 µg/ml collagen and 0.1 U/ml thrombin for 30 min at 37°C. Subsequently, cells were centrifuged at 12,600 rpm for 30 min and the supernatant was collected. Freshly isolated human neutrophils were plated at 10^5 on poly-L-lysine–coated Fluoro-Dishes and incubated for 15 min at 37°C with platelets in the presence of 100 nM PMA and 20 µg/ml aprotinin. Short-term incubation with PMA does not lead to NET formation.

Thereafter, cells were fixed with 4% PFA in PBS. Cells were washed three times with PBS and then incubated with blocking buffer (5% fish gelatin, 5% donkey serum, 1% BSA, and 0.05% Tween 20 in PBS, pH 7.4) for 30 min at 37°C. Cells were stained with a primary antibody directed against H2A-H2B-DNA complexes (1:10 in blocking buffer), which was generated as previously described (Losman et al., 1992), for 30 min at 37°C. Cells were washed three times with PBS before applying a secondary antibody goat anti–mouse Cy3-labeled (1:300 in blocking buffer) for 2 h at 37°C (Invitrogen). Cells were washed three times with PBS and two times with aqua dest. before an incubation with DAPI (Sigma-Aldrich) to detect DNA. Cells were washed two times with aqua dest. before microscopic analysis, and the samples were pretreated with 10 U/ml DNase1 or vehicle as control.

For visualization of colocalization of NETs and FXII, human neutrophils were plated at 5×10^4 on poly-L-lysine–coated FluoroDishes. After 30 min of co-incubation with 5×10^5 platelets in the presence of 100 nM PMA and 20 µg/ml aprotinin in Hepes buffer, 100 nmol FXII was added for additional 15 min at 37°C in the presence of zinc. The negative control did not contain FXII. Then cells were fixed in 4% PFA, and the nucleic acids were stained by Sytox green (Invitrogen) as described in the manual. The nonspecific bindings were blocked, and afterward 5 mg/ml of a mouse anti–human FXII antibody (ab1007; Abcam) was added for 1 h, followed by a secondary anti–mouse Alexa Fluor 594 (Invitrogen) antibody for 30 min at 2 mg/ml in PBS.

Visualization was performed by confocal microscopy using an LSM 510 META (Carl Zeiss), based on an inverted Axiovert 200 MOT microscope.

A 63× magnification was obtained with the use of Plan-Apochromat lenses (1.4 NA, oil immersion). Image acquisition was performed using LSM Browser software (Carl Zeiss), and for the image processing Photoshop (Adobe) was used.

Factor XIIa formation assay. Neutrophils (N) were only preactivated with 100 nM PMA (control) or co-incubated with platelets (P/N) for 15 min at 37°C in the presence of 8 µg/ml collagen. Subsequently, they were incubated for 30 min with H2A-H2B-DNA–specific antibody or control IgG (each 20 µg/ml). Then the samples were mixed with 50 nM FXII in the presence of 50 µM $ZnCl_2$ and a chromogenic substrate S2302. The absorption of the samples was measured photometrically at 405 nm. FXII in 50 µM $ZnCl_2$ and S2302 (Co), preactivated platelets alone (P), and preactivated neutrophils alone (N) served as controls

RT-PCR. RNA was isolated from the whole IVC using the NucleoSpin RNA XS kit (Macherey-Nagel) according to the manufacturer's instructions. Template cDNA was synthesized from 2 µg total RNA using the High Capacity cDNA Archive kit (Applied Biosystems) and applied in SYBR Green assays performed on a GeneAmp 7700 Sequence Detection System (Applied Biosystems). The murine sequences of CXCL1, CXCL5, CCL2, IL6, and P-selectin were detected by QuantiTect Primer Assays (QIAGEN). Cycling conditions were 50°C for 2 min and 95°C for 15 min, followed by 40 cycles of denaturation at 95°C for 15 s, and annealing and elongation at 60°C for 60 s. Gene expression ratios for each sample (regulation factors and standard deviation) were calculated using the ddCt method (Livak and Schmittgen, 2001) and normalized against β-actin. Experiments were performed as triplicate, including non-reverse transcription and nontemplate controls. Dissociation analysis confirmed the specificity of the reaction.

FACS. Whole blood from each animal was collected from the facial vein and assayed for flow cytometry by standard techniques. Neutrophils were stained using PE-labeled rat anti–mouse Ly6G (clone 1A8; BD), and monocytes were detected by double-positive staining with rat anti–mouse CD115-PE (clone AFS98; eBioscience) and rat anti–mouse CD11b-APC (clone M1/70; eBioscience). Antibody specificity was verified using an appropriate isotype-labeled antibody (anti–rat IgG2a or anti–rat IgG2b). Erythrocytes were depleted from the preparations with BD FACS lysing solution (BD). Flow cytometric measurement was performed on a FACSCalibur (BD) using CellQuest software.

Statistical analysis. All data are shown as mean ± SEM, unless indicated otherwise. Thrombus weight was tested for normal distribution using the Kolmogorov-Smirnov test and the independent samples Student's t test was performed to compare groups (SPSS). More than two groups were compared using the ANOVA-LSD post hoc test. Parameters like number of adherent cells/mm² or aggregation area were analyzed by unpaired Student's t test. For flow velocity data, the paired Students t test was used. A value of P < 0.05 was considered significant.

Online supplemental material. Video 1 shows an i.v. contrast-enhanced computed tomography image of a thrombosed IVC in vivo. Video 2 illustrates the recruitment of leukocytes to the IVC. Video 3 shows crawling neutrophils on the venous vessel wall. Video 4 visualizes the recruitment of neutrophils in LysM-eGFP mice to the endothelium. Video 5 shows monocytes and neutrophils in CX3CR1-eGFP mice attached to the vessel wall. Video 6 demonstrates the 3D structure of NETs in the thrombus. Video 7 is a time-lapse movie demonstrating extracellular DNA originating from neutrophils in vivo inside the IVC. Video 8 is a time-lapse movie showing platelets and neutrophils forming a thrombus at the vessel wall. Video 9 illustrates in 3D how neutrophils and platelets cover the endothelial surface in vivo. Video 10 shows how platelets recruit neutrophils to the developing thrombus in a time-lapse movie. Table S1 lists the antibodies used for the experiments. Online supplemental material is available at http://www.jem .org/cgi/content/full/jem.20112322/DC1

JEM

REFERENCES

Ammollo, C.T., F. Semeraro, J. Xu, N.L. Esmon, and C.T. Esmon. 2011. Extracellular histones increase plasma thrombin generation by impairing thrombomodulin-dependent protein C activation. *J. Thromb. Haemost.* 9:1795–1803. http://dx.doi.org/10.1111/j.1538-7836.2011.04422.x

Angelillo-Scherrer, A., P. de Frutos, C. Aparicio, E. Melis, P. Savi, F. Lupu, J. Arnout, M. Dewerchin, M. Hoylaerts, J. Herbert, et al. 2001. Deficiency or inhibition of Gas6 causes platelet dysfunction and protects mice against thrombosis. *Nat. Med.* 7:215–221. http://dx.doi.org/10.1038/84667

Brill, A., T.A. Fuchs, A.K. Chauhan, J.J. Yang, S.F. De Meyer, M. Köllnberger, T.W. Wakefield, B. Lämmle, S. Massberg, and D.D. Wagner. 2011. von Willebrand factor–mediated platelet adhesion is critical for deep vein thrombosis in mouse models. *Blood.* 117:1400–1407. http://dx.doi.org/10.1182/blood-2010-05-287623

Brinkmann, V., U. Reichard, C. Goosmann, B. Fauler, Y. Uhlemann, D.S. Weiss, Y. Weinrauch, and A. Zychlinsky. 2004. Neutrophil extracellular traps kill bacteria. *Science.* 303:1532–1535. http://dx.doi.org/10.1126/science.1092385

Bucek, R.A., M. Reiter, P. Quehenberger, and E. Minar. 2002. C-reactive protein in the diagnosis of deep vein thrombosis. *Br. J. Haematol.* 119:385–389. http://dx.doi.org/10.1046/j.1365-2141.2002.03886.x

Cheng, Q., E.I. Tucker, M.S. Pine, I. Sisler, A. Matafonov, M.F. Sun, T.C. White-Adams, S.A. Smith, S.R. Hanson, O.J. McCarty, et al. 2010. A role for factor XIIa–mediated factor XI activation in thrombus formation in vivo. *Blood.* 116:3981–3989. http://dx.doi.org/10.1182/blood-2010-02-270918

Clark, S.R., A.C. Ma, S.A. Tavener, B. McDonald, Z. Goodarzi, M.M. Kelly, K.D. Patel, S. Chakrabarti, E. McAvoy, G.D. Sinclair, et al. 2007. Platelet TLR4 activates neutrophil extracellular traps to ensnare bacteria in septic blood. *Nat. Med.* 13:463–469. http://dx.doi.org/10.1038/nm1565

Clausen, B.E., C. Burkhardt, W. Reith, R. Renkawitz, and I. Förster. 1999. Conditional gene targeting in macrophages and granulocytes using LysMcre mice. *Transgenic Res.* 8:265–277. http://dx.doi.org/10.1023/A:1008942828960

Cohen, A.T., G. Agnelli, F.A. Anderson, J.I. Arcelus, D. Bergqvist, J.G. Brecht, I.A. Greer, J.A. Heit, J.L. Hutchinson, A.K. Kakkar, et al; VTE Impact Assessment Group in Europe (VITAE). 2007. Venous thromboembolism (VTE) in Europe. The number of VTE events and associated morbidity and mortality. *Thromb. Haemost.* 98:756–764.

Day, S.M., J.L. Reeve, B. Pedersen, D.M. Farris, D.D. Myers, M. Im, T.W. Wakefield, N. Mackman, and W.P. Fay. 2005. Macrovascular thrombosis is driven by tissue factor derived primarily from the blood vessel wall. *Blood.* 105:192–198. http://dx.doi.org/10.1182/blood-2004-06-2225

Diaz, J.A., A.E. Hawley, C.M. Alvarado, A.M. Berguer, N.K. Baker, S.K. Wroblreski, T.W. Wakefield, B.R. Lucchesi, and D.D. Myers Jr. 2010. Thrombogenesis with continuous blood flow in the inferior vena cava. A novel mouse model. *Thromb. Haemost.* 104:366–375. http://dx.doi.org/10.1160/TH09-09-0672

Eitzman, D.T., R.J. Westrick, E.G. Nabel, and D. Ginsburg. 2000. Plasminogen activator inhibitor-1 and vitronectin promote vascular thrombosis in mice. *Blood.* 95:577–580.

Esmon, C.T. 2009. Basic mechanisms and pathogenesis of venous thrombosis. *Blood Rev.* 23:225–229. http://dx.doi.org/10.1016/j.blre.2009.07.002

Faust, N., F.Varas, L.M. Kelly, S. Heck, and T. Graf. 2000. Insertion of enhanced green fluorescent protein into the lysozyme gene creates mice with green fluorescent granulocytes and macrophages. *Blood.* 96:719–726.

Fuchs, T.A., A. Brill, D. Duerschmied, D. Schatzberg, M. Monestier, D.D. Myers Jr., S.K. Wroblreski, T.W. Wakefield, J.H. Hartwig, and D.D. Wagner. 2010. Extracellular DNA traps promote thrombosis. *Proc. Natl. Acad. Sci. USA.* 107:15880–15885. http://dx.doi.org/10.1073/pnas.1005743107

Furie, B., and B.C. Furie. 2007. In vivo thrombus formation. *J. Thromb. Haemost.* 5:12–17. http://dx.doi.org/10.1111/j.1538-7836.2007.02482.x

Gailani, D., N.M. Lasky, and G.J.J. Broze Jr. 1997. A murine model of factor XI deficiency. *Blood Coagul. Fibrinolysis.* 8:134–144. http://dx.doi.org/10.1097/00001721-199703000-00008

Garcia-Romo, G.S., S. Caielli, B. Vega, J. Connolly, F. Allantaz, Z. Xu, M. Punaro, J. Baisch, C. Guiducci, R.L. Coffman, et al. 2011. Netting neutrophils are major inducers of type I IFN production in pediatric systemic lupus erythematosus. *Sci. Transl. Med.* 3:ra20. http://dx.doi.org/10.1126/scitranslmed.3001201

Geerts, W.H., K.I. Code, R.M. Jay, E. Chen, and J.P. Szalai. 1994. A prospective study of venous thromboembolism after major trauma. *N. Engl. J. Med.* 331:1601–1606. http://dx.doi.org/10.1056/NEJM199412153312401

Griep, M.A., K. Fujikawa, and G.L. Nelsestuen. 1985. Binding and activation properties of human factor XII, prekallikrein, and derived peptides with acidic lipid vesicles. *Biochemistry.* 24:4124–4130. http://dx.doi.org/10.1021/bi00336a047

Heit, J.A. 2008. The epidemiology of venous thromboembolism in the community. *Arterioscler. Thromb. Vasc. Biol.* 28:370–372. http://dx.doi.org/10.1161/ATVBAHA.108.162545

Heit, J.A., C.E. Kobbervig, A.H. James, T.M. Petterson, K.R. Bailey, and L.J. Melton III. 2005. Trends in the incidence of venous thromboembolism during pregnancy or postpartum: a 30-year population-based study. *Ann. Intern. Med.* 143:697–706.

Hughes, R.J., R.J. Hopkins, S. Hill, M. Weatherall, N. Van de Water, M. Nowitz, D. Milne, J. Ayling, M. Wilsher, and R. Beasley. 2003. Frequency of venous thromboembolism in low to moderate risk long distance air travellers: the New Zealand Air Traveller's Thrombosis (NZATT) study. *Lancet.* 362:2039–2044. http://dx.doi.org/10.1016/S0140-6736(03)15097-0

Jung, S., J. Aliberti, P. Graemmel, M.J. Sunshine, G.W. Kreutzberg, A. Sher, and D.R. Littman. 2000. Analysis of fractalkine receptor CX(3)CR1 function by targeted deletion and green fluorescent protein reporter gene insertion. *Mol. Cell. Biol.* 20:4106–4114. http://dx.doi.org/10.1128/MCB.20.11.4106-4114.2000

Kanaji, T., S. Russell, and J. Ware. 2002. Amelioration of the macrothrombocytopenia associated with the murine Bernard-Soulier syndrome. *Blood.* 100:2102–2107. http://dx.doi.org/10.1182/blood-2002-03-0997

Konings, J., J.W. Govers-Riemslag, H. Philippou, N.J. Mutch, J.I. Borissoff, P. Allan, S. Mohan, G. Tans, H. Ten Cate, and R.A. Ariëns. 2011. Factor XIIa regulates the structure of the fibrin clot independently of thrombin generation through direct interaction with fibrin. *Blood.* 118:3942–3951. http://dx.doi.org/10.1182/blood-2011-03-339572

Livak, K.J., and T.D. Schmittgen. 2001. Analysis of relative gene expression data using real-time quantitative PCR and the 2(-Δ Δ C(T)) Method. *Methods.* 25:402–408. http://dx.doi.org/10.1006/meth.2001.1262

Losman, M.J., T.M. Fasy, K.E. Novick, and M. Monestier. 1992. Monoclonal autoantibodies to subnucleosomes from a MRL/Mp(-)+/+ mouse. Oligoclonality of the antibody response and recognition of a determinant composed of histones H2A, H2B, and DNA. *J. Immunol.* 148:1561–1569.

Mackman, N. 2008. Triggers, targets and treatments for thrombosis. *Nature.* 451:914–918. http://dx.doi.org/10.1038/nature06797

Mammen, E.F. 1992. Pathogenesis of venous thrombosis. *Chest.* 102:640S–644S. http://dx.doi.org/10.1378/chest.102.6.640S

Manly, D.A., J. Boles, and N. Mackman. 2011. Role of tissue factor in venous thrombosis. *Annu. Rev. Physiol.* 73:515–525. http://dx.doi.org/10.1146/annurev-physiol-042210-121137

Massberg, S., G. Enders, R. Leiderer, S. Eisenmenger, D. Vestweber, F. Krombach, and K. Messmer. 1998. Platelet-endothelial cell interactions during ischemia/reperfusion: the role of P-selectin. *Blood.* 92:507–515.

Massberg, S., K. Brand, S. Grüner, S. Page, E. Müller, I. Müller, W. Bergmeier, T. Richter, M. Lorenz, I. Konrad, et al. 2002. A critical role of platelet adhesion in the initiation of atherosclerotic lesion formation. *J. Exp. Med.* 196:887–896. http://dx.doi.org/10.1084/jem.20012044

Massberg, S., M. Gawaz, S. Grüner, V. Schulte, I. Konrad, D. Zohlnhöfer, U. Heinzmann, and B. Nieswandt. 2003. A crucial role of glycoprotein VI for platelet recruitment to the injured arterial wall in vivo. *J. Exp. Med.* 197:41–49. http://dx.doi.org/10.1084/jem.20020945

Massberg, S., L. Grahl, M.L. von Bruehl, D. Manukyan, S. Pfeiler, C. Goosmann, V. Brinkmann, M. Lorenz, K. Bidzhekov, A.B. Khandagale, et al. 2010. Reciprocal coupling of coagulation and innate immunity via neutrophil serine proteases. *Nat. Med.* 16:887–896. http://dx.doi.org/10.1038/nm.2184

Moll, S., and N. Mackman. 2008. Venous thromboembolism: a need for more public awareness and research into mechanisms. *Arterioscler. Thromb. Vasc. Biol.* 28:367–369. http://dx.doi.org/10.1161/ATVBAHA.108.163097

Myers, D. Jr., D. Farris, A. Hawley, S. Wrobleski, A. Chapman, L. Stoolman, R. Knibbs, R. Strieter, and T. Wakefield. 2002. Selectins influence thrombosis in a mouse model of experimental deep venous thrombosis. *J. Surg. Res.* 108:212–221. http://dx.doi.org/10.1006/jsre.2002.6552

Pal, P.K., T. Starr, and M.M. Gertler. 1983. Neutralization of heparin by histone and its subfractions. *Thromb. Res.* 31:69–79. http://dx.doi.org/10.1016/0049-3848(83)90008-7

Parry, G.C., J.H. Erlich, P. Carmeliet, T. Luther, and N. Mackman. 1998. Low levels of tissue factor are compatible with development and hemostasis in mice. *J. Clin. Invest.* 101:560–569. http://dx.doi.org/10.1172/JCI814

Pauer, H.U., T. Renné, B. Hemmerlein, T. Legler, S. Fritzlar, I. Adham, W. Müller-Esterl, G. Emons, U. Sancken, W. Engel, and P. Burfeind. 2004. Targeted deletion of murine coagulation factor XII gene-a model for contact phase activation in vivo. *Thromb. Haemost.* 92:503–508.

Pawlinski, R., M. Tencati, T. Holscher, B. Pedersen, T. Voet, R.E. Tilley, P. Marynen, and N. Mackman. 2007. Role of cardiac myocyte tissue factor in heart hemostasis. *J. Thromb. Haemost.* 5:1693–1700. http://dx.doi.org/10.1111/j.1538-7836.2007.02649.x

Pawlinski, R., J.G. Wang, A.P. Owens III, J. Williams, S. Antoniak, M. Tencati, T. Luther, J.W. Rowley, E.N. Low, A.S. Weyrich, and N. Mackman. 2010. Hematopoietic and nonhematopoietic cell tissue factor activates the coagulation cascade in endotoxemic mice. *Blood.* 116:806–814. http://dx.doi.org/10.1182/blood-2009-12-259267

Payling Weight, H., S.B. Osborn, and D. Edmonds. 1951. Effect of postoperative bed rest and early ambulation on the rate of venous blood-flow. *Lancet.* 257:22–25. http://dx.doi.org/10.1016/S0140-6736(51)93496-4

PEP-Group. 2000. Prevention of pulmonary embolism and deep vein thrombosis with low dose aspirin: Pulmonary Embolism Prevention (PEP) trial. *Lancet.* 355:1295–1302. http://dx.doi.org/10.1016/S0140-6736(00)02110-3

Ramacciotti, E., S. Blackburn, A.E. Hawley, F. Vandy, N. Ballard-Lipka, C. Stabler, N. Baker, K.E. Guire, J.E. Rectenwald, P.K. Henke, et al. 2011. Evaluation of soluble P-selectin as a marker for the diagnosis of deep venous thrombosis. *Clin. Appl. Thromb. Hemost.* 17:425–431. http://dx.doi.org/10.1177/1076029611405032

Reinhardt, C., M.L. von Brühl, D. Manukyan, L. Grahl, M. Lorenz, B. Altmann, S. Dlugai, S. Hess, I. Konrad, L. Orschiedt, et al. 2008. Protein disulfide isomerase acts as an injury response signal that enhances fibrin generation via tissue factor activation. *J. Clin. Invest.* 118:1110–1122.

Roger, V.L., A.S. Go, D.M. Lloyd-Jones, R.J. Adams, J.D. Berry, T.M. Brown, M.R. Carnethon, S. Dai, G. de Simone, E.S. Ford, et al; American Heart Association Statistics Committee and Stroke Statistics Subcommittee. 2011. Heart disease and stroke statistics—2011 update: a report from the American Heart Association. *Circulation.* 123:e18–e209. http://dx.doi.org/10.1161/CIR.0b013e3182009701

Roumen-Klappe, E.M., M.C. Janssen, J. Van Rossum, S. Holewijn, M.M. Van Bokhoven, K. Kaasjager, H. Wollersheim, and M. Den Heijer. 2009. Inflammation in deep vein thrombosis and the development of post-thrombotic syndrome: a prospective study. *J. Thromb. Haemost.* 7:582–587. http://dx.doi.org/10.1111/j.1538-7836.2009.03286.x

Sevitt, S. 1970. Organic canalisation and vascularisation of deep vein thrombi studied with dyed-micropaque injected at necropsy. *J. Pathol.* Pi.

Sevitt, S. 1974. The structure and growth of valve-pocket thrombi in femoral veins. *J. Clin. Pathol.* 27:517–528. http://dx.doi.org/10.1136/jcp.27.7.517

Silverstein, M.D., J.A. Heit, D.N. Mohr, T.M. Petterson, W.M. O'Fallon, and L.J. Melton III. 1998. Trends in the incidence of deep vein thrombosis and pulmonary embolism: a 25-year population-based study. *Arch. Intern. Med.* 158:585–593. http://dx.doi.org/10.1001/archinte.158.6.585

Smeeth, L., C. Cook, S. Thomas, A.J. Hall, R. Hubbard, and P. Vallance. 2006. Risk of deep vein thrombosis and pulmonary embolism after acute infection in a community setting. *Lancet.* 367:1075–1079. http://dx.doi.org/10.1016/S0140-6736(06)68474-2

Stewart, G.J., W.G. Ritchie, and P.R. Lynch. 1974. Venous endothelial damage produced by massive sticking and emigration of leukocytes. *Am. J. Pathol.* 74:507–532.

Varma, M.R., A.J. Varga, B.S. Knipp, P. Sukheepod, G.R. Upchurch, S.L. Kunkel, T.W. Wakefield, and P.K. Henke. 2003. Neutropenia impairs venous thrombosis resolution in the rat. *J. Vasc. Surg.* 38:1090–1098. http://dx.doi.org/10.1016/S0741-5214(03)00431-2

Wakefield, T.W., R.M. Strieter, C.A. Wilke, A.M. Kadell, S.K. Wrobleski, M.D. Burdick, R. Schmidt, S.L. Kunkel, and L.J. Greenfield. 1995. Venous thrombosis-associated inflammation and attenuation with neutralizing antibodies to cytokines and adhesion molecules. *Arterioscler. Thromb. Vasc. Biol.* 15:258–268. http://dx.doi.org/10.1161/01.ATV.15.2.258

Wang, X., P.L. Smith, M.Y. Hsu, M.L. Ogletree, and W.A. Schumacher. 2006. Murine model of ferric chloride-induced vena cava thrombosis: evidence for effect of potato carboxypeptidase inhibitor. *J. Thromb. Haemost.* 4:403–410. http://dx.doi.org/10.1111/j.1538-7836.2006.01703.x

Ward, C.M., T.J. Tetaz, R.K. Andrews, and M.C. Berndt. 1997. Binding of the von Willebrand factor A1 domain to histone. *Thromb. Res.* 86:469–477. http://dx.doi.org/10.1016/S0049-3848(97)00096-0

Warlow, C., D. Ogston, and A.S. Douglas. 1976. Deep venous thrombosis of the legs after strokes: Part 2-Natural history. *BMJ.* 1:1181–1183. http://dx.doi.org/10.1136/bmj.1.6019.1181

Wright, H.P., S.B. Osborn, and M. Hayden. 1952. Venous velocity in bed-ridden medical patients. *Lancet.* 2:699–700. http://dx.doi.org/10.1016/S0140-6736(52)91318-4

Zhou, J., L. May, P. Liao, P.L. Gross, and J.I. Weitz. 2009. Inferior vena cava ligation rapidly induces tissue factor expression and venous thrombosis in rats. *Arterioscler. Thromb. Vasc. Biol.* 29:863–869. http://dx.doi.org/10.1161/ATVBAHA.109.185678